ABSTRACT

RESEARCH AND DEVELOPMENT FOR THE MU2E EXTINCTION MONITOR

Casey B. Mott, M.S.
Department of Physics
Northern Illinois University, 2016
David Hedin, Director

Mu2e is a planned experiment to search for flavor violating conversion from a muon to an electron. The experiment will use a pulsed 8 GeV proton beam to produce muons which will then stop in an aluminum target. Mu2e will search for the $\mu^- + Al \rightarrow e^- + Al$ process. For Mu2e, an extinction rate of 10^{-10} is required to reduce the backgrounds to an acceptable level. Extinction is the ratio of the amount of protons striking the production target between beam pulses to the number striking it during the beam pulse. One of the backgrounds, off-target interactions, was simulated using G4beamline and Fermilab's Grid setup to confirm that an extinction rate of 10^{-10} is possible.

The extinction level will be measured by the extinction monitor which will include scintillation counters read out by photomultiplier tubes. In order to build a beam time profile, low fake responses (after pulses) are needed in the photomultiplier tubes. This thesis determines the best combination of resistors, voltage, and other components that provide the lowest after pulse rate.

NORTHERN ILLINOIS UNIVERSITY
DE KALB, ILLINOIS

MAY 2016

RESEARCH AND DEVELOPMENT FOR THE MU2E EXTINCTION MONITOR

BY

CASEY B. MOTT

A THESIS SUBMITTED TO THE GRADUATE SCHOOL
IN PARTIAL FULFILLMENT OF THE REQUIREMENTS
FOR THE DEGREE
MASTER OF SCIENCE

DEPARTMENT OF PHYSICS

Thesis Director:
David Hedin

ACKNOWLEDGEMENTS

I would first like to thank my adviser, Dr. David Hedin, for his guidance through this master's thesis.

Also, this project would not have been possible without the help of Alexander Dychkant, who provided endless insights and stories, and Eric Johnson, who wrote the initial programming.

I want to extend my gratitude to the other members of my thesis committee, Dr. Vishnu Zutshi and Dr. Gerald C. Blazey, for their time and input.

I would like to thank Dr. Peter Kasper, Dr. Andrei Gaponenko, Dr. Eric Prebys, as well as all the members of the Mu2E collaboration for their support while working on this project.

I would like to thank all the faculty, staff, and my fellow students in the NIU Physics Department.

I want to acknowledge Eric Apgar, for his continual support and editing, my sister, for constantly pushing me to do better, and my parents, for always encouraging me to do what I love.

I want to thank my wife for being my constant soundboard, and giving me the patience and love to finish this master's thesis. I could not have done it without her.

Finally, I want to acknowledge the National Science Foundation for their funding and support.

DEDICATION

To the Future

TABLE OF CONTENTS

LIST OF TABLES

LIST OF FIGURES

Figure Page

Figure Page

CHAPTER 1

INTRODUCTION

Particle physics aims to understand the universe around us. Within particle physics there are three basic categories, often called the energy, cosmic, and intensity frontiers. Each category uses a different set of techniques and tools to ultimately answer the same fundamental questions. The intensity frontier looks for fundamental interactions beyond the Standard Model by detecting extremely rare processes. This is done by utilizing ultra-sensitive detectors to measure a high intensity beam of particles that produces a large number of interactions. There are several divisions in the intensity frontier that are currently investigating rare processes and decays, such as [1]

- K, B, and D meson decay
- Neutrino oscillation and mass measurements
- Measurements of electric dipole moments
- Charged lepton flavor violation

The Mu2e Experiment at Fermilab studies charged lepton flavor-violation ($\mu^- + Al \rightarrow e^- + Al$ process) by utilizing top of the line accelerators, detectors, superconducting magnets, electronics, and other equipment to maximize sensitivity to such a rare process. Unfortunately, there are background sources that can lead to fake conversion electrons during the measurement period. Because of this, the experiment design includes a dedicated extinction monitor to measure extinction at the 10^{-10} level in a few hours of sampling. Extinction is the ratio of the amount of protons striking the production target between beam pulses to the

number striking it during the beam pulse. The setup will include scintillating counters read out by photomultiplier tubes in order to create a statistical profile. Additionally, this will be used to accurately model backgrounds due to out-of-time protons as a function of time for a given run period. This thesis explores research and development for the extinction monitor. Two items were studied: simulating off-target interactions using G4beamline and Fermilab's Grid setup to confirm that an extinction rate of 10^{-10} is possible, and determining the best combination of resistors, voltage, and other components that provide the lowest after pulse rate in a photomultiplier tube.

CHAPTER 2
PARTICLE PHYSICS AND CHARGED LEPTON FLAVOR VIOLATIONS

2.1 Introduction and Motivation

Ancient Greek philosophers introduced the idea that all matter was constructed from atoms, the smallest division matter could be divided into. The word atom comes from the Greek word atomos, "a" meaning not and "tomos" meaning cuttable. Unfortunately, their ideas were founded in theological and philosophical reasoning rather than experimentation and evidence. Consequently, their viewpoint of what atoms looked like and how they behaved was disproven. However, their basic atomic theory was shown to be true and further developed in the late 1700's and early 1800's (most notably by John Dalton) to explain why elements always react in ratios of small whole numbers (the law of multiple proportions).

Physicists later found that the atoms of different elements, thought to be a single fundamental unit, actually consisted of protons, neutrons, and electrons. The question then arose whether these particles could be further subdivided. The theories and discoveries of physicists since the 1930's resulted in a breakthrough of the fundamental structure of matter: everything in the universe is made from a few basic building blocks called subatomic particles, and is governed by four fundamental forces. Scientists' best understanding of how these particles interact with each other and three of the four forces is described using the Standard Model.

2.2 Standard Model

The Standard Model states that all matter is constructed from subatomic particles: leptons, quarks, and other particles that mediate interactions between these groups. This model is depicted clearly by Figure 2.1 [2].

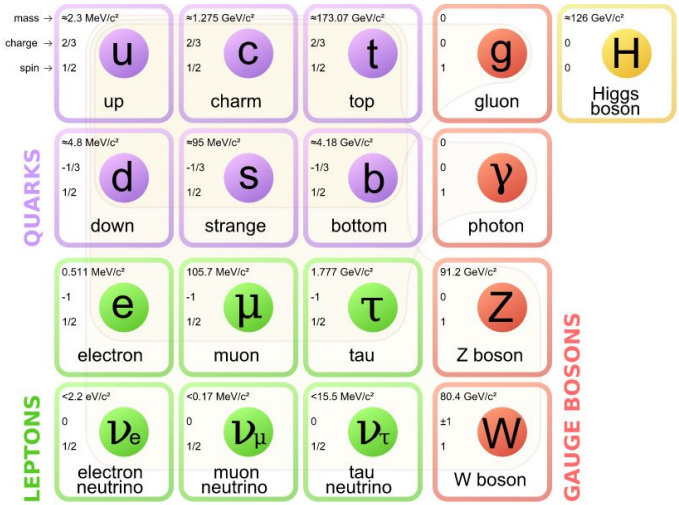

Figure 2.1: The Standard Model

Currently, the Standard Model depicts three distinct sets of particles; the fermions, gauge bosons, and the Higgs boson. The fermions consist of the first three columns, or generations, in Figure 2.1. Each fermion carries a half integer spin and is further categorized into two groups based on how they behave. These two groups consist of six quarks (up, down, charm, strange, top, bottom), and six leptons (electron, electron neutrino, muon, muon neutrino, tau, tau neutrino).

The defining property of the quarks is that they carry color charge, which means they interact via the strong interaction. A phenomenon called color confinement results in quarks being very strongly bound to one another. Quarks form three sets of particles, either color-neutral composite particles (hadrons), a quark and an antiquark (mesons), or three quarks

(baryons). The familiar proton and the neutron are the two baryons having the smallest mass. Quarks also carry electric charge and weak isospin. Therefore, they interact with other fermions both electromagnetically and through the the weak interaction.

The remaining six fermions do not carry color charge and are called leptons. The three neutrinos do not carry electric charge either, so their motion is only influenced by the weak nuclear force, which makes them difficult to detect. However, electrons, muons, and taus carry an electric charge, allowing them to all interact electromagnetically.

Each particle in a generation has less mass than the corresponding particles of higher generations. The first generation (first column of Figure 2.1) of particles do not decay. This allows all atoms to be made up of atomic nuclei composed of up and down quarks with electrons orbiting around the nucleus. Additionally, neutrinos for all three generations do not decay, and rarely interact with other particles [3]. On the other hand, fundamental particles in the second and third generation decay with very short half lives and are observed only in high-energy environments.

Gauge bosons are defined as the force carriers that arbitrate the strong, weak, and electromagnetic interactions. Each boson has an integer spin of one, meaning they do not follow the Pauli exclusion principle that constrains the fermions. Therefore, there is not a theoretical limit on how many bosons can inhabit a given volume. The different types of bosons are described below along with Figure 2.2 which provides an overall summary [4].

- The W+, W, and Z gauge bosons mediate the weak interactions between particles of different flavors (all quarks and leptons). They are massive, with the Z being more massive than the W.

- Photons mediate the electromagnetic force between electrically charged particles. The photon is massless and is well described by the theory of quantum electrodynamics.

- The gluons mediate the strong interactions between color charged particles (the quarks). Gluons are massless. Because the gluons have an effective color charge, they can also interact among themselves. The gluons and their interactions are described by the theory of quantum chromodynamics.

The four fundamental forces of nature[28]

Property/Interaction	Gravitation	Weak	Electromagnetic	Strong	
		(Electroweak)		Fundamental	Residual
Acts on:	Mass - Energy	Flavor	Electric charge	Color charge	Atomic nuclei
Particles experiencing:	All	Quarks, leptons	Electrically charged	Quarks, Gluons	Hadrons
Particles mediating:	Graviton	W^+ W^- Z^0	γ	Gluons	Mesons

Figure 2.2: The Fundamental Forces

The Higgs boson has an exclusive role in the Standard Model which explains why the other fundamental particles, except gluons and photons, are massive. Specifically, the Higgs boson explains why the W and Z bosons are very heavy, while the photon has no mass. Because the Higgs boson is very massive itself, and decays almost immediately, only the highest energy particle accelerators could detect and record it. In the summer of 2012, the ATLAS and CMS collaborations of the Large Hadron Collider (LHC) at CERN tentatively confirmed that the Higgs boson existed. Later, in 2013, other channels confirmed the discovery of the Higgs boson [5].

2.2.1 Why CLFV?

The muon, along with the muon neutrino, belongs to one of three flavors of leptons (the other flavors being the electron and the tau with their respective neutrinos). In almost all interactions, the number of leptons in a given flavor is conserved. So far, the only exception is when a neutrino from one flavor oscillates into another flavor, such as a tau neutrino

oscillating into a muon neutrino. However, a lepton flavor violation has never been observed in the decay of a charged lepton, such as a muon. The Standard Model incorporates the conservation of lepton flavor and the violation of flavor by neutrino oscillations, but it is not fully understood why these two events occur. In fact, there is no known reason, such as symmetry, as to why there is lepton flavor conservation. Since most physics models beyond the Standard Model readily allow charged lepton flavor violation (CLFV), the failure to detect any violations so far puts constraints on these models. With lepton flavor properties being so instrumental to our comprehension of lepton behavior, and very little being known about these properties, there is intense experimental interest in discovering or setting new limits on the occurrence of CLFV. Currently, there are several experiments already planned or under way.

2.3 Previous or Ongoing Experiments

For the sake of efficiency, many experiments choose to study the decay of muons as opposed to the heavier tau. Muons live longer before they decay into lighter particles and are easier to produce in large quantities. Many experiments have already been preformed on CLFV with muons. These experiments were generally using a muon beam incident on a stationary target to generate an interaction. The SINDRUM II experiment was conducted at the Paul Scherrer Institute (PSI) in Switzerland and looked for $\mu - e$ conversion in gold nuclei ($\mu^- Au \rightarrow e^- Au$). The MEG experiment, also conducted at PSI, and the MEGA experiment, conducted at the Los Alamos National Laboratory Meson Physics Facility (LAMPF), both searched for $\mu^+ \rightarrow e^+\gamma$. The TRIUMF experiment preformed several searches for $\mu - e$ conversion in various atomic nuclei. Alternately, CLFV can also be probed in collider

experiments such as BaBar at SLAC and Belle at KEK [6]. The branching ratio for these six experiments are displayed in Table 2.1

Table 2.1: Experiments CLFV Branching Limits

Process	*UpperLimit*	*Experiment*
$\mu^- Pb \rightarrow e^- Pb$	7.0×10^{-13}	SINDRUM II
$\mu^- Au \rightarrow e^- Au$	5.7×10^{-13}	MEG
$\mu^+ \rightarrow e^+ \gamma$	1.2×10^{-11}	MEGA
$\mu^+ \rightarrow e^+ \gamma$	4.9×10^{-10}	TRIUMF
$\tau \rightarrow \mu\gamma$	4.5×10^{-8}	Belle
	4.4×10^{-8}	BaBar
$\tau \rightarrow e\gamma$	3.3×10^{-8}	Belle
	1.2×10^{-7}	BaBar

2.4 Overview of Mu2e

The Mu2e experiment will be 10,000 times more sensitive than previous experiments looking for muon-to-electron conversion. This will be done by repurposing the particle accelerator already on Fermilab's campus that previously produced anti-protons for the Tevatron experiments. For details of the Mu2e experiment, see reference [7].

2.4.1 Accelerator Facilities

This experiment requires a high intensity proton beam in order to produce the needed muons. This is done by the Fermilab Booster. The Booster is a circular accelerator, 500 feet in diameter, that uses magnets to bend electrically charged particles in a circular path. Every time the particles travel around the ring they are accelerated due to the electric fields

present, increasing their energy each time. The proton beam of 4×10^{12} protons per batch travels around the Booster about 20,000 times, until its energy is raised to 8 GeV (eight billion electron volts) [8]. An overview of the Mu2e complex can be seen in Figure 2.3.

After reaching the required energy, the protons are sent from the Booster to the Recycler Ring via the MI-8 beam line. Once in the Recycler, the proton beam undergoes time and spatial structuring where each proton batch is separated into four bunches with 400 ns between each bunch. From the Recycler, the protons are extracted to the Delivery Ring where they will be sent to the muon area in a pulsed fashion. This allows particles from the first batch to decay before the next batch is sent to the muon area. The time between the bunches is the revolution period of the Delivery Ring, or 1695 ns, as seen in Figure 2.4. Once in the muon area, the protons will react with a target and the resulting particles will travel through three different solenoids to finish the experiment: the production, transport, and detector solenoids.

2.4.2 Solenoids

The Mu2e experiment contains three distinct sections of superconducting solenoids as seen in Figure 2.5.

The proton beam will first enter the Production Solenoid at an angle where it hits the production target. The particles produced in the target travel through the Transport Solenoid to the Detector Solenoid region. Some of these particles will be incident on the stopping target where the tracker and calorimeter will detect whether there is any muon to electron conversion. Each of the solenoids were designed to maximize the number of muons to reach the stopping target per proton on the production target.

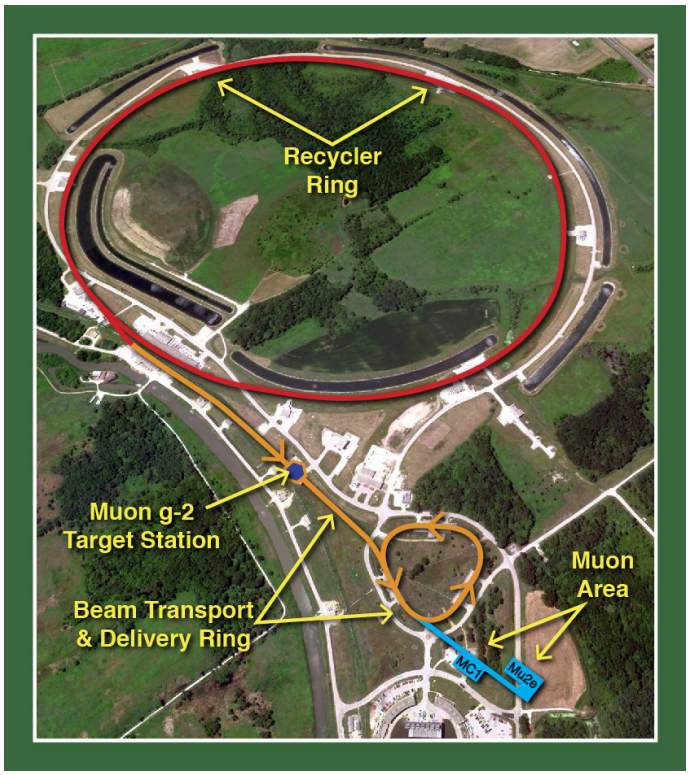

Figure 2.3: Overhead View of Fermilab's Mu2e Layout

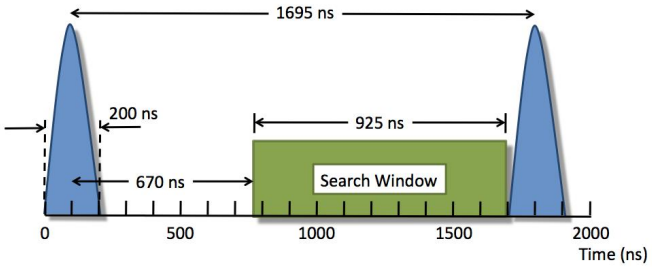

Figure 2.4: Proton bunch separation with time and search windows.

There are three different coordinate systems used by Mu2e. The Mu2e coordinate system has an origin in the center of the Transport Solenoid with the z axis parallel to the Production and Detector Solenoidal axes. The x and x axis are in their normal horizontal and vertical alignment. The detector and tracker coordinate systems have axes parallel to the Mu2e coordinate system, except the origin is at the center of their respective solenoid. With

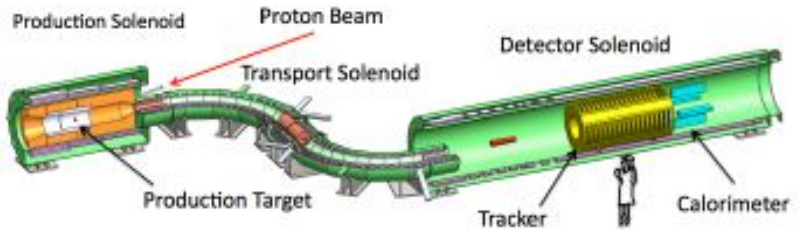

Figure 2.5: Solenoids in the Muon Area.

relation to the Mu2e coordinate system, the detector coordinate system is located at -3904.0, 0.0, 12000 mm, and the tracker coordinate system is located at -3904.0, 0.0, 10200 mm.

2.4.2.1 Production Solenoid

On its journey, the proton beam first enters the Production Solenoid, colliding with a cylindrical tungsten target with 3.15 mm radius and 180 mm length centered at 3904.0, 0.0, -6164.5 mm in the Mu2e coordinate system. The primary purpose of the Production Solenoid is to provide muons for the Mu2e experiment through the proton beam's interaction with the production target. This is coupled with axially graded magnetic fields which range from 2.5 Tesla to 4.6 Tesla and direct the particles with the appropriate momentum range to be accelerated toward the Transport Solenoid. Many of the pions created from the production target interaction will decay to muons along their trip towards the Transport Solenoid. For Mu2e, the expected production rate is 0.0016 muons stopped on the Aluminum target per proton on the production target. In addition to this main function, the Production Solenoid provides secondary particle radiation protection, and also allows the proton beam to exit without interfering with the magnet shield. A cross-sectional view of the Production Solenoid can be seen in Figure 2.6 [7].

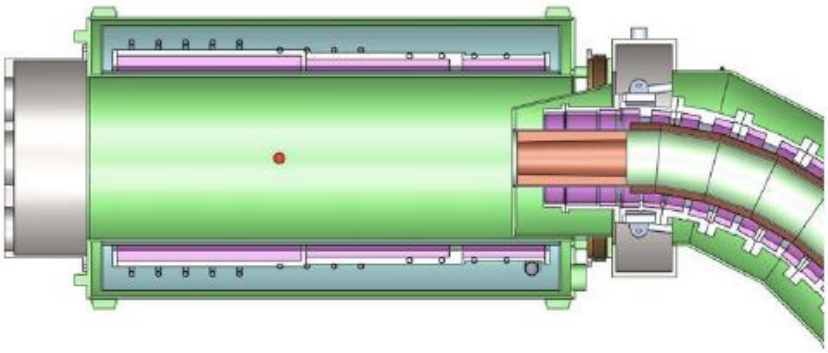

Figure 2.6: Cross-sectional view of the Production Solenoid.

2.4.2.2 Transport Solenoid

The Transport Solenoid is essential for carrying muons from the Production Solenoid to the Detector Solenoid. This solenoid maximizes the muon yield by directing the muons that are within the proper momentum range toward the stopping target located in the Detector Solenoid. The Transport Solenoid consists of several superconducting solenoids that form a reverse S-shape, as can be seen in Figure 2.7. The initial bend in the Transport Solenoid exists to reject neutral and high energy charged particles. Altogether, there are three collimators and absorbers: TS1, TS3, and TS5. These prevent positively charged particles from entering the Detector Solenoid. In the most recent design, TS2 and TS4 collimators are no longer present [7].

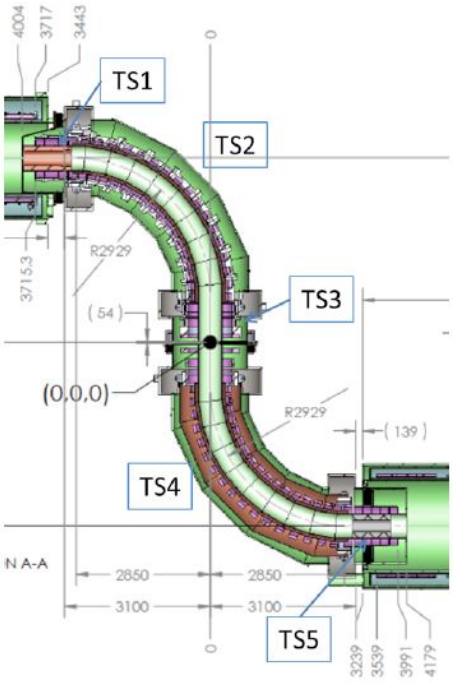

Figure 2.7: Cross-sectional top view of the Transport Solenoid. TS2 and TS4 are no longer present

2.4.2.3 Detector Solenoid

The scatter and random energy of the original production particles are now carefully selected for observing the muon-to-electron conversion. A low energy muon beam will enter the Detector Solenoid after traveling through the Transport Solenoid. The Detector Solenoid has both graded and uniform magnetic fields as shown in Figure 2.8. A graded field exists across the stopping target with a range from 2T to 1T. This field sends particles created in the stopping target towards the tracker if it has downstream momentum and rejects any particles created with upstream momentum. About 40% of the incoming muon beam will come to rest in the aluminum stopping target and be captured by the aluminum nuclei. These muons will either decay in orbit or undergo nuclear capture, with a small fraction

possibly undergoing direct conversion. The other 60% of the muons will be stopped by the Muon Beam Stop.

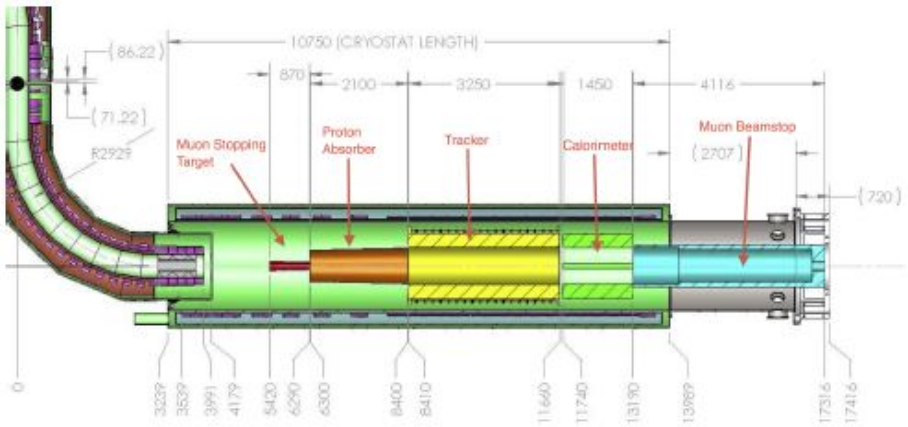

Figure 2.8: Cross-sectional top view of the Detector Solenoid with Stopping Target, Proton Absorber, Tracker, Calorimeter, and Muon Beam Stop labeled.

Downstream of the stopping target lies the cylindrical shell polyethylene proton absorber. This acts to reduce the number of protons that enter the detector region. The actual Mu2e detector is made up of two parts, the tracker and calorimeter, that reside in a uniform magnetic field. The tracker consists of 22,000 drift tubes aligned in the x-y plane that measure the momentum of the electrons passing through the drift tubes. These have been optimized to distinguish between the converted electrons and the electrons that result from the muons decaying in orbit. The calorimeter is a system of scintillating crystals and photodetectors that provide information such as position, energy, and timing of particles leaving tracks in the tracker. Together, these two instruments will be able to tell if a muon decays into an electron in the stopping target and measure the energy of the electron.

Further downstream from the calorimeter is the Muon Beam Stop. Besides capturing excess muons, the Muon Beam Stop serves as shielding for components within the detector from particles produced from the muon capture. It also protects the outside world from radiation. The Muon Beam Stop is essential in preventing the backscatter of photons and

electrons from interacting with the target tracker and calorimeter. Minimizing this backscatter provides more accurate measurements by keeping the detector from measuring the same electron more than once. Finally, the Muon Beam Stop serves to absorb neutrons which are appreciable background in the cosmic ray veto counters located outside the Detector Solenoid.

2.4.3 Stopping Target

The Muon Stopping Target is a central component of the Mu2e experiment. Muons captured by the stopping target lose some energy and form muonic atoms, which can potentially undergo neutrino-less conversion of muons to electrons. The stopping target is designed to maximize the number of stopped muons while minimizing the amount of material a converted electron must travel through to reach the detector further downstream. The new configuration is thirty-four aluminum foils of 100 μm thickness with a uniform radius of 75 mm in the downstream direction as seen in Figure 2.9.

The entire apparatus is centered at 0.0, 0.0, -6129.0 mm ranging from z = -6529 mm to z = -5729 mm in the detector coordinate system. Each layer of the aluminum foil is separated by 50 mm along the axis of the detector solenoid. The Muon Stopping Target is supported by a series of thin tungsten wires attached to each layer so it is suspended perfectly aligned with the incoming muon beam.

The material chosen for the Muon Stopping Target is aluminum with 99.99% purity. The motivations for choosing aluminum include many factors such as muon lifetime, muon conversion rate, converted electrons energy, and related backgrounds. The muon lifetime decreases with increasing atomic number (Z). For aluminum, the stopped muon lifetime is 864 ns and the $\mu - e$ conversion energy is 104.97 MeV. This muon lifetime is roughly half

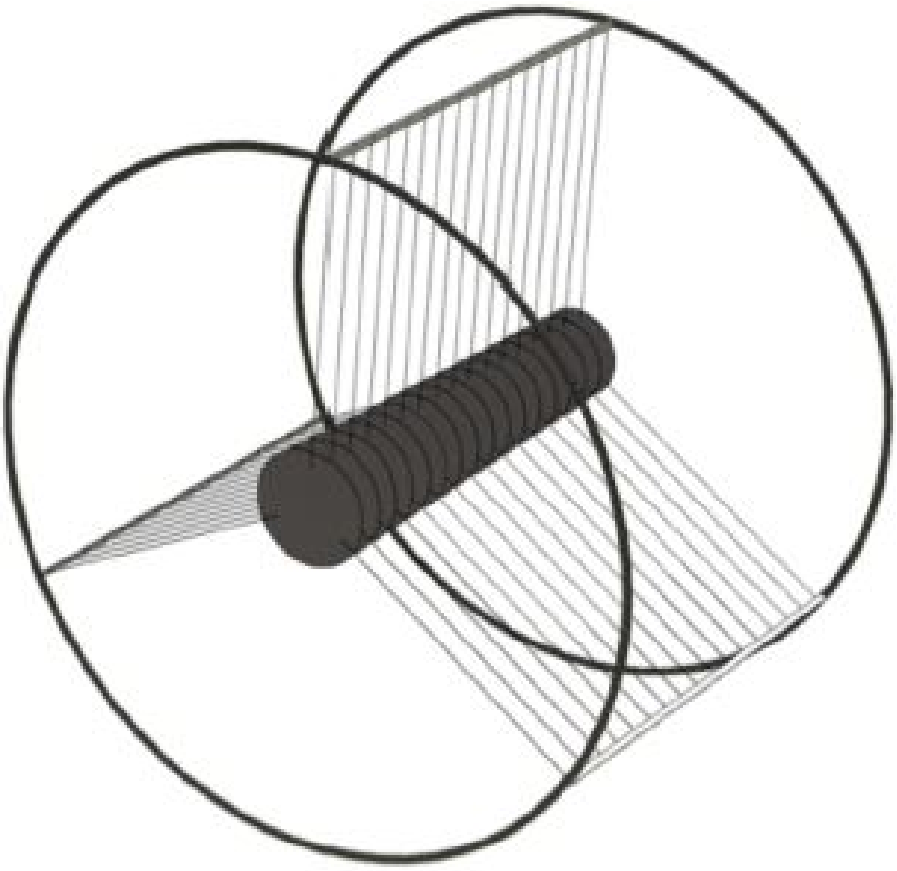

Figure 2.9: Standard Mu2e stopping target with tungsten support structures

the time between proton bunches. This reduces the number of background events directly related to the muon beam occurring during the detector live gate time when the electron conversion process takes place. The muon conversion rate increases with increasing Z, up until selenium, where it then begins to decrease.

2.4.3.1 Energy Loss in the Stopping Target

The magnetic field in the Transport and Detector Solenoids cause charged particles to travel in helical paths as given by

$$R = \frac{p\tau}{qB} \tag{2.1}$$

where R is the radius of the helix, $p\tau$ is the transverse momentum, q is the charge, and B is the magnetic field. When a charged particle interacts with matter it will lose energy as given by the Bethe-Bloch equation [12].

$$\frac{dE}{dx} = \frac{\rho K z^2 Z}{A\beta^2}\left(\frac{1}{2}ln\left(\frac{2m_e c^2\beta^2\gamma^2 T_{max}}{I^2}\right) - \beta^2\right) \tag{2.2}$$

Where ρ is the density of the material, K = 0.307 MeV = $4\pi N_A \tau_e^2 m_e c^2$, z is the incident particle's charge, Z is the atomic number of the material, A is the atomic mass number of the material, β is the velocity divided by the speed of light, m_e is the electron mass, γ is the Lorentz factor, I is the mean excitation energy of the material, and T_{max} is the maximum kinetic energy that can be imparted to a free electron in a collision. As the muons travel through the stopping target they will lose energy. However, because of their helical trajectory, the muons are not guaranteed to transverse every layer of the stopping target. This makes determining the exact amount of energy lost from interacting with a material very difficult to predict.

CHAPTER 3

EXTINCTION MONITOR

One of the consequences of the finite muon lifetime is the production of backgrounds that could potentially "fake" physics events in the detector. A significant amount of backgrounds are produced by secondary beam particles (pions) that reach the detector region in a time interval shortly after protons hit the production target. To reduce these events, the Mu2e experiment uses a pulsed proton beam operating at approximately 0.6 MHz. The search window to look for muon tracks is 670 ns after each proton pulse, as seen in Figure 2.4. A total measurement period of 700 - 1700 ns after injection matches the 0.88 ms lifetime of muonic aluminum. A complete schematic of the proton pulse, pion arrival/decay time, muon arrival time, and muon decay time is shown in Figure 3.1.

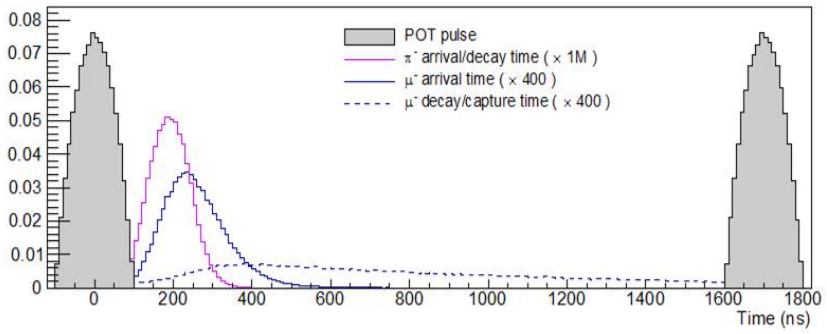

Figure 3.1: Histogram depicting time windows for protons, pions, and muons.

Backgrounds can also be produced by protons hitting the production target during or slightly before the search window. Beam extinction is a ratio of the amount of protons striking the production target *between* beam pulses to the number striking it *during* the beam pulses. Beam extinction is required to be approximately 10^{-10} in order to reduce the

backgrounds to an acceptable level. The Mu2e proton beam cycle and the delayed search window allows for the effective elimination of prompt backgrounds when the number of protons between pulses is suppressed to the required level.

The beam extinction will be achieved in two steps:

- The technique for generating the required bunch structure in the Recycler Ring naturally leads to a high level of extinction. There is a fast "kicker" which transfers the proton beam from the Recycler to the Delivery Ring that should preserve this level of extinction. Altogether, an extinction of 10^{-5} is expected as the proton beam is extracted and delivered.

- The beam line from the Delivery Ring to the production target has a set of AC oscillating dipoles that sweep out-of-time protons into a system of collimators. This should achieve an additional extinction of 10^{-7} or better.

Direct extinction measurements are difficult since there is a high rate of particles. Mu2e focuses on measuring particles scattered from the proton beam and production target interaction. Using a detector with a small effective acceptance and a good time resolution, a statistical profile can be built of the out-of-time particles over many bunches.

There are two time scales of interest to the extinction monitor. Although the total time of the experiment is important, a much shorter time period (about an hour) has been chosen so that any problems that arise can be detected quickly before a significant amount of data is lost. This will be the high precision portion measurements, about 10^{-10}. In order to compensate for subtle problems that could arise with the extinction in the delivery ring, a much shorter time scale is also used with a precision of 10^{-5}.

For the high precision measurements, the experiment has a dedicated production target extinction monitor, also called a target monitor. The target extinction monitor design consists of a momentum filter made up of collimators and a permanent dipole magnet, a mag-

netic spectrometer with planes of silicon strips, scintillating trigger counters with a dipole magnet, and a range stack that helps establish how many muons are in the in-time beam and the out-of-time beam. It also includes a collimator located upstream of the primary beam line. This collimator eliminates beam halo that would otherwise interact with the Production Solenoid and become a source of background events. All of these components, as well as their placement, can be seen in Figure 3.2 and 3.3

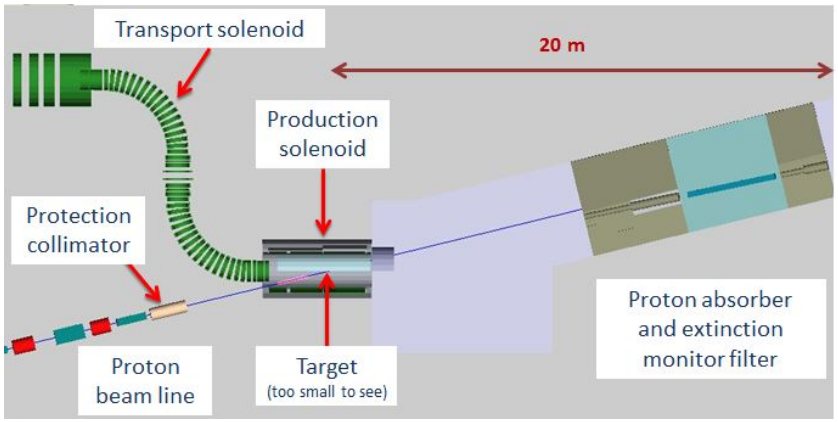

Figure 3.2: Location of the extinction monitor

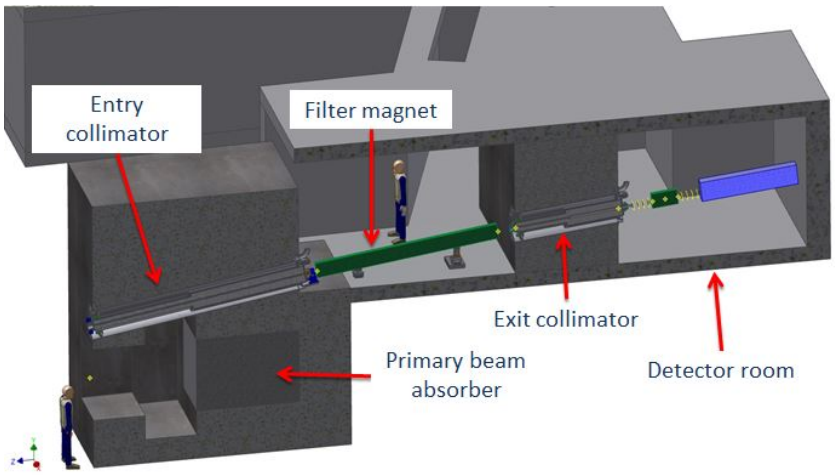

Figure 3.3: The components of the extinction monitor

3.1 Backgrounds to $\mu^- + Al \rightarrow e^- + Al$

For Mu2e sensitivity there are a number of processes that can mimic a muon to electron conversion signal. The overall design of the Mu2e experiment is based on reducing these potential backgrounds. Backgrounds result primarily from: pion contamination, decay-in-orbit (DIO), radiative muon capture (RMC), cosmic rays, and off-target interactions.

3.1.1 Radiative Pion Capture

Pions can produce backgrounds when they are captured in the stopping target or surrounding material and produce high energy photons through radiative pion capture (RPC).

$$\pi^- N \rightarrow \gamma N \tag{3.1}$$

If the photon then converts internally, an electron near the conversion energy can be produced. In addition, the photon can convert in the stopping material to create an electron-positron pair where the outgoing electron is also near the conversion energy.

$$\pi^- N \rightarrow e^+ e^- N \tag{3.2}$$

The RPC background is suppressed by using a pulsed proton beam. The search for converted electrons is delayed until nearly 100% of the pions have decayed or been annihilated.

3.1.2 Decay In Orbit

A free muon decays with a peak probability of maximum energy at half the muon rest energy (well below the energy of a converted electron). However, if the muon is bound in the atomic orbit, the outgoing electron can exchange momentum with the nucleus, thereby increasing its energy to levels comparable to a converted electron. The probabilities and spectrum of electron energies can be modeled with the Michel spectrum, as illustrated in Figure 3.4

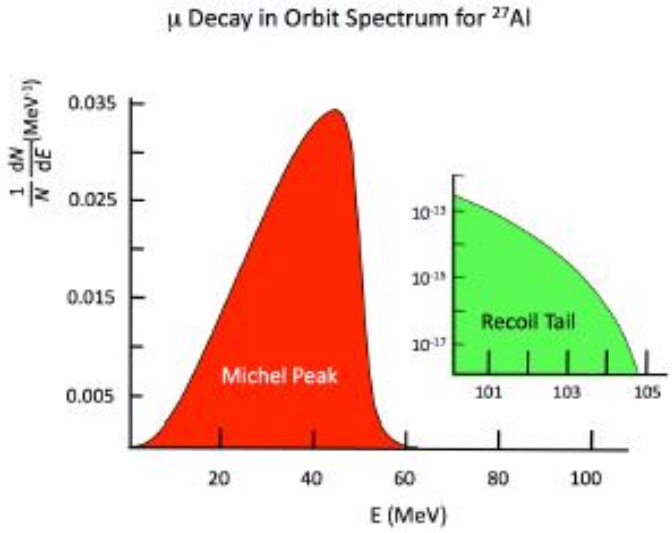

Figure 3.4: The electron energy spectrum from muon decay-in-orbit in aluminum.

Because of the rapid decrease in the DIO rate as the electron energy increases, the background can be suppressed with excellent resolution of the electron momentum.

3.1.3 Radiative Muon Capture

Radiative muon capture on the nucleus of the stopping target creates photons that can either convert internally or produce an electron-positron pair with energy near the conversion electron energy.

$$\mu^- Al \rightarrow \gamma \nu Mg \tag{3.3}$$

Ideally, the stopping target is chosen so that the minimum masses of the daughter nuclei are all a couple of MeV/c^2 above the rest mass of the stopping target nucleus. This would push the RMC photon energy below the conversion electron energy. For aluminum, the RMC final electron energy is 101.9 MeV which is just slightly lower than the converted electron energy of 105 MeV. The rate of radiative muon capture is not well known for medium mass nuclei, but the electrons that result cannot exceed the kinematic endpoint for the energy of a radiated photon. The currently planned energy resolution for the converted energy peak will make this background negligible.

3.1.4 Cosmic Rays

Cosmic rays (electrons, muons, and photons) have the potential to be a source of electrons that will have energy near the converted electron energy. If their trajectories look like they originated in the stopping target, then they can fake a muon to electron conversion. Cosmic Ray Vetos (CRV) and shielding can greatly reduce these backgrounds; however, it will be useful to identify any incoming cosmic ray particles so that Mu2e can reject these events. A

table of simulated Mu2e background sources and their estimated yield can be seen in Table 3.5

Table 3.1: A list of background processes and their estimated yield.

Category	Background Process	Estimated yield (events)
Intrinsic	Muon decay-in-orbit (DIO)	0.199±0.092
	Muon capture (RMC)	$0.00^{+0.004}_{-0.000}$
Late Arriving	Pion capture (RPC)	0.023±0.006
	Muon decay-in-flight (μ-DIF)	<0.003
	Pion decay-in-flight (π-DIF)	0.001± <0.001
	Beam electrons	0.003±0.001
Miscellaneous	Antiproton induced	0.047±0.024
	Cosmic ray induced	0.092±0.020
	Total	0.37±0.10

3.1.5 Off-Target Interaction

This last background is potentially the most misleading source of fake physics events since it cannot be measured when the beam is offline. When the out-of-time beam enters the production solenoid, interactions can occur off-target that generate signals in the extinction monitor. The off-target background depends largely on the orientation of the filter compared to the distribution of out-of-time beam interactions inside the heat and radiation shield that surrounds the target. Though not well understood, this alignment is based upon the transverse structure of the out-of-time-beam. In order to restrict the transverse size of the beam, collimators are placed where the beam enters the heat and radiation shield, so that the beam fits well within the beam entry opening. These collimators prevent the beam from interacting in the heat and radiation shield and significantly reduce the off-target interaction.

To determine how many of the off-target interactions would create fake physics events, a simulation was run and is further discussed in chapter 4.

3.2 Filter Magnet

As can be seen in Figure 3.3, a permanent dipole magnet rests between two collimators that transports charged particles to the extinction monitor detector room. In order to maximize the signal rate, simulations determined that the particles must have an average momentum of 4.2 GeV/c. Because of its orientation, the magnet also serves to remove unwanted background sources from low energy neutral particles, such as photons and neutrons.

With a weight of 4,286 lbs and length of 3,683 mm, the filter magnet sits on its own kinematic mount that is free to adjust in roll, pitch, and yaw. Below the ball and socket joint, there are vertically threaded rods that can manipulate the height of the magnet. The socket itself is mounted on a horizontal slide that adjusts the transverse positioning of the magnet. The idea behind the kinematic mount is that any adjustment can be made without interfering with any other adjustments, or causing strain to build up in the structure. This concept has been employed on E760 and most recently on the LBNE target and horn modules.

3.3 Upstream/Downstream Collimators

The first component of the extinction monitor is an entry collimator that selects secondary particles produced off of the production target. It is oriented in line with the beam axis in order to maximize signal rate, but is at a large angle so as to avoid the proton beam absorber.

The collimators are steel pipes filled with concrete and then surrounded by a larger pipe called a fixed liner. Custom spherical bearings will be able to adjust the collimators anywhere

inside of the fixed liner pipe, changing the pitch and yaw angles of the beam channel. Since the radiation levels will be to high near the entry collimator too allow human access, two circular cams that are driven by shafts running around the outside of the fixed liner up into the magnet room will be installed. The pitch and yaw angles can be individually adjusted through these cams. The entry collimator weighs 2,022 lbs, is 4.28625 m long, and has a beam aperture of 50 mm.

After the filter magnet is an exit collimator that is embedded in a two-meter thick concrete wall that shields the detector room from radiation from the particles that did not make it through the collimators. The exit collimator has all of the same features as the entry collimator, save the cam drive, since both ends of the exit collimator are accessible. The beam channel also becomes larger halfway through the collimator, from 50 mm aperture to 75 mm, to reduce the amount of interactions that occur near the detector room. The exit collimator weighs 1,015 lbs and is 2.203 m long.

3.4 Proton Beam Absorber

A proton beam absorber will stop the unspent proton beam and secondary particles so that they do not leave the Production Solenoid. The absorber consists of a steel core (1.5 m $\times$ 1.5 m $\times$ 2 m) with a concrete shielding around it (3.5 m $\times$ 3.5 m $\times$ 5 m). The core is surrounded by at least 1 m of concrete on all 6 sides. There is a 1.5 m $\times$ 1.5 m opening towards the beam and also a 2.5 m $\times$ 2.5 m $\times$ 1 m neutron absorber trap to keep any secondary particles generated by the spent proton beam in the core from escaping downstream towards the end of the Production Solenoid.

In the event that the target is missed (or during pre-targeting beam tests) the absorber is able to accept the entire beam power - approximately 8 kW. The beam absorber will

also be able to accept the total number of protons required by Mu2e (3.6×10^{20} over 3 - 4 years plus an additional overhead) without replacement during the life of the experiment [13]. The transverse dimensions of the absorber are consistent with the beam properties after accounting for the divergence of the beam and the distance from the target. A cross sectional view of the proton beam absorber, along with its temperature distribution, is shown in Figure 3.5.

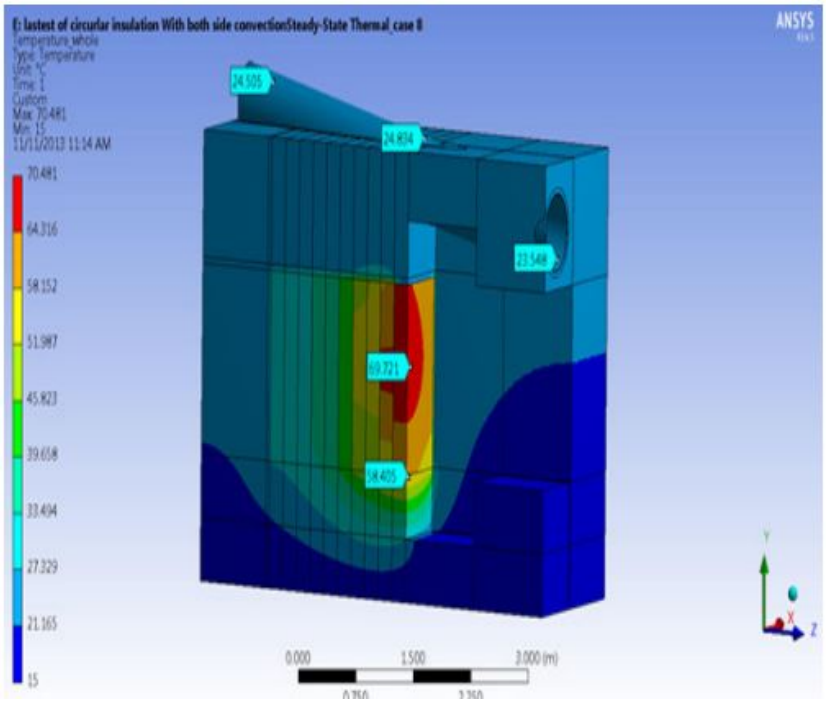

Figure 3.5: Cross sectional view of proton beam absorber along with temperature distribution.

3.5 Detector Room

The Mu2e extinction monitor detector consists of two sensor stacks with four pixel planes each. A permanent magnet sits in between the stacks to allow reconstruction of the track momentum, as seen in Figure 3.6.

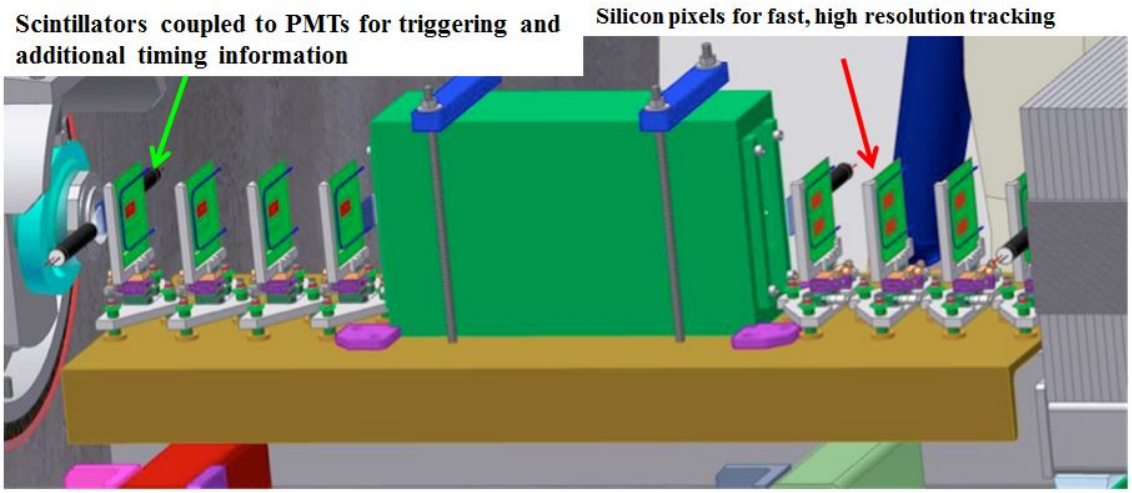

Figure 3.6: Triggers, pixels and spectrometer magnet on the channel table.

Trigger counters serve to provide a trigger for the pixel detectors for the out-of-time particles. Between proton pulses, it is only expected to see a few particles per hour. The trigger counters also serve as a time stamp for when out-of-time particles are observed with a resolution of about a nanosecond. Three trigger counters are used with each set of pixel counters. A trigger will require a coincidence in two out of the three counters.

The counters are 5 mm thick and slightly larger than the pixel detectors. In essence, a trigger counter consists of a scintillator and a photomultiplier tube (PMT). The scintillator used will be BC-404 and emits light when ionized by radiation. A Hamamatsu PMT (or equivalent) will detect this light, multiply the current, and read out to a discriminator board.

3.5.1 Photomultipler Tubes

Photomultiplier tubes are vacuum tubes that are extremely sensitive to light. These detectors can multiply a current produced by incident light by as much as 100 million times. The combination of high gain, low noise, high frequency response, and large area of collection make them ideal for the extinction monitor.

PMT's are typically constructed with a glass housing holding a photocathode, dynodes, and an anode, as seen in Figure 3.7.

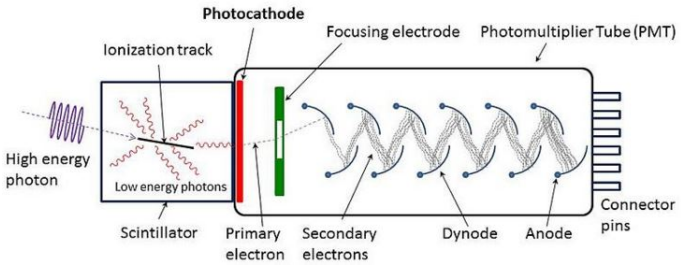

Figure 3.7: PMT with primary components labeled.

Incident photons strike a photocathode material - a thin conducting layer on the inside of the entry window of the device. As a consequence of the photoelectric effect, electrons are ejected from the surface. These electrons are directed toward the electron multiplier, which multiplies the number of electrons present through the process of secondary emission [14].

The electron multiplier is made up of a number of electrodes called dynodes, as shown in Figure 3.8. Each dynode is held at a more positive potential than the preceding one. A primary electron leaves the photocathode with energy close to that of the incoming photon. Due to the present electric field, the primary electrons accelerate toward the first dynode. Upon striking, more low energy electrons are emitted. In turn, these electrons accelerate toward the second dynode. The dynode chain is constructed such that a cascade occurs with an exponentially increasing number of electrons being produced at each stage. When this large number of electrons reach the anode, a current pulse that is proportional to the energy of the original photon is generated. This current can be easily detected and displayed through an oscilloscope.

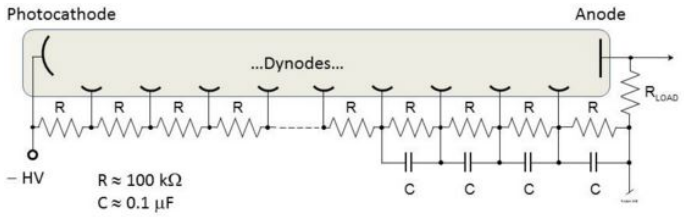

Figure 3.8: Example of a typical dynode chain.

3.6 Upstream Extinction Monitor

To reiterate, there will be a target monitor downstream of the production target to monitor the protons striking the target for the final extinction measurement. The monitor will have an integration time of an hour and rely on the beam interaction with the target to provide a measure of extinction level. Because the target extinction monitor relies on the production target and will be located downstream of the AC oscillating dipoles that exist between the Delivery Ring and the Production Solenoid, another monitor is proposed to measure extinction upstream of the AC Dipole on a faster time scale and be used for beam tune-up. This monitor is not in the Mu2e baseline but may be funded by other means.

A small thin film obstruction, 5 μm Ti, will be placed in the path of the beam. Telescopes, out of the path of the beam, will be used to detect Cherenkov light from secondary particles produced by the beam-foil interaction. The key requirement is that the detector has a short time resolution compared to the proton pulse length and also has a low fake rate [15].

The four telescopes will have four Cherenkov counters each that are read out by a PMT to a waveform digitizer that will allow the time structure of the Cherenkov light to be analyzed. Instead of scintillators, quartz radiators will be connected to the PMT's. Quartz radiators were chosen because they do not contain intrinsic after pulses, there is a very fast response time, and they are blind to soft particles. The telescopes will be located 2 m downstream of the foil outside of the beamline and positioned in a straight line to its beam point intersection.

The telescopes are tuned in such a way that scattering from the in-time protons will not cause saturation.

A beam time profile will be built by integrating over several bunches. The difficulties with this profile come from the need for good time resolution, the ability of the photo detector to withstand high rates, a large dynamic range, and low fake responses (such as after pulses in the photomultiplier tubes used in coincidence) [16].

CHAPTER 4

SIMULATING EXTINCTION MONITOR BACKGROUND

The Mu2e collaboration uses several simulation software packages to design and optimize the components of the experiment. In particular, the Mu2e simulation software is built on the GEANT4 solid geometry and physics interaction software library. Using this framework, all components of the Mu2e experiment can be constructed in the simulation environment. Within the framework, particle interactions with matter are simulated, and track reconstruction is conducted. G4beamline, specifically designed for simulating beamlines, is a single particle tracking and simulation program by Tom Roberts of Muons, Inc. to run GEANT4 [17]. G4beamline v2.16 was used to simulate an out-of-time proton beam incident on the target to detect fake target extinction model signal rate per proton hitting the target.

The signal rate can be approximated by assuming a bunch rate of 0.6 MHz at a duty factor of 33%. This leads to 2×10^{16} in-time protons per hour. For an extinction of 10^{-10}, there will only be 2×10^{6} out-of-time protons per hour. A signal detection rate in the target monitor system of 10^{-6} events per proton-on-target gives approximately 2 out-of-time events detected per hour. This acceptance for a normal 8 GeV beam on target has been previously estimated using G4beamline. This section estimates the rate in the extinction monitor for inter-bunch out-of-time protons which are bent by the AC dipole when the magnetic field is on, and could be a background to the true out-of-time protons which remain in the beam.

Besides G4beamline, Fermilab's Grid setup was needed to run the large number of events in a timely manner. Grid computing is a form of distributed computing in which multiple clusters of nodes work together to complete tasks. Physicists submit jobs, computer programs

that physicists use to extract physics results from data, to the grid. The grid determines which resources are free and uses those nodes to process the job [18].

After accessing Fermilab's network, four setups need to be completed: Mu2e setup, Root setup, Grid setup, and G4beamline setup. The Mu2e setup allows the user to have access to all the Mu2e software on the cluster, including G4beamline. Root setup is needed in order to make plots or histograms in post processing. Grid setup simply allows the user to access Fermilab's worker nodes and submit jobs to them. Finally, the G4beamline setup specifies what version of G4beamline the user wants to work in.

4.1 Coordinates

The simulations that were run used a coordinate system where the (0,0) point was centered on the production target. The z-axis had its 0.0 point at the end of the Production Solenoid. The z-axis runs the length of the solenoid system so the positive z-axis is downstream towards the Detector Solenoid, and the negative z-axis is by the target extinction monitor. The x and y axes remain in their normal horizontal and vertical alignment with respect to the initial proton beam as seen in Figure 4.1.

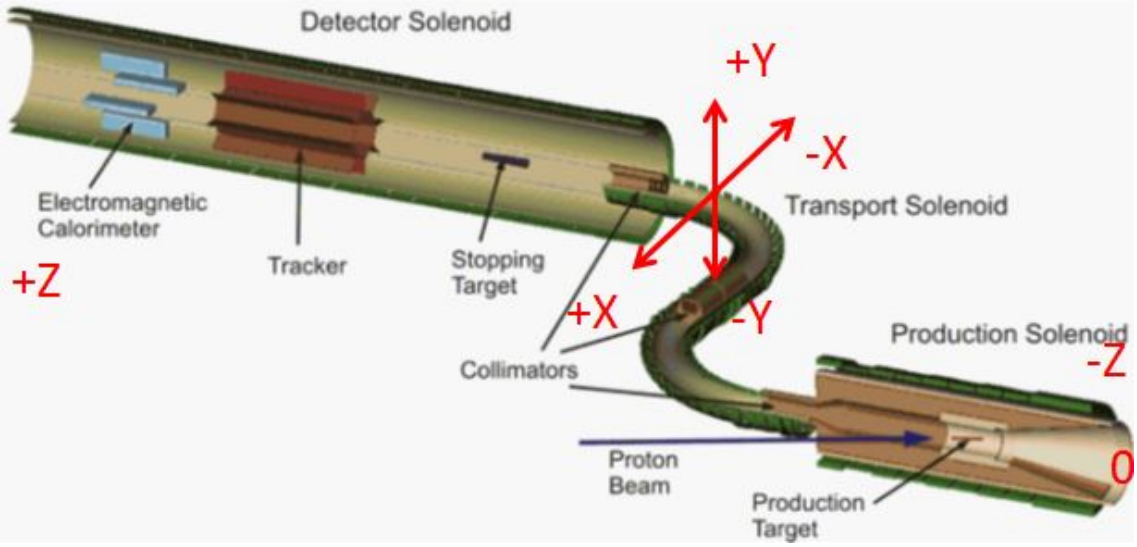

Figure 4.1: Crossectional view showing the x, y, and z axes. The 0.0 point is at the end of the Production Solenoid.

4.2 Simulation Details

To begin our simulation, an out-of-time beam was needed. The distribution was generated using a G4beamline model of the M4 beam line from the extinction AC dipole to the end of the final focus, including the extinction collimator. The beam distribution assumed a normalized 95% emittance of 15 pi-mm-mr in the vertical (non-bend) plane and a uniform normalized emittance of 30 pi-mm-mr in the horizontal (bend) plane. This is based on simulations of beam extraction from the Delivery Ring.

The AC dipole bend magnet strength was set to the minimum angle required to achieve "complete extinction" of the beam $\delta = 2$ [19]. Simulations were run on 100 nodes, which generated 1,000,000 events each. Results of the simulation were stored to Ntuples in standard G4beamline format and tracks which survived to the end were used as the input for subsequent simulation.

Of the 10^8 events, approximately 3,000 were incident on the target. In order to generate the "worst case scenario", these 3,000 were the basis for the out-of-time beam that was later sent through G4beamline. The 3,000 events were saved to the file ntuplecopy.C. Figure 4.2 shows the initial x, y, z, p_x, p_y, p_z for the original 3,000 events. The y-axis is the frequency, showing the number of events, and the x-axis is displayed in either millimeters or MeV/c.

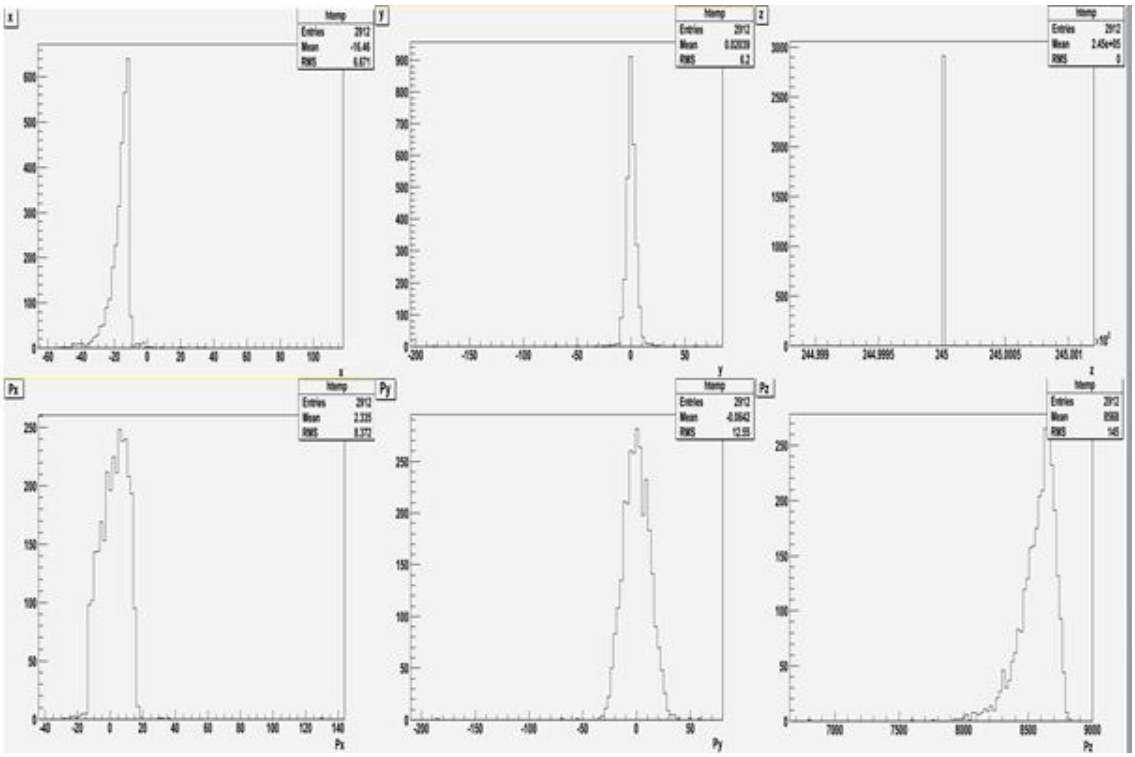

Figure 4.2: The x, y, z, p_x, p_y, p_z of the original 3,000 events that were incident on the target. The x-axis is in millimeters for x, y, z and in MeV/c for p_x, p_y, p_z.

In order to create the out-of-time beam, the 3,000 events were run through MakeBeam.C, a function that created three ranges around the x, y, p_x, p_y, and p_z coordinates for each particle. The first range had a radius of 5 mm, the second range had a radius of 10 mm, and the third range had a radius of 40 mm. A random particle was chosen to be first. In order to preserve particle density, the minimum range that contained at least one other particle was

found. The difference between the target particle and its nearest neighbors was calculated. If the range contained more than one particle, then the distance between them was normalized. A new particle was created within a plus or minus range of this normalized distance. To achieve the statistics desired, this was done to each of the original 3,000 particles 1,000 times. Figure 4.3 shows the x, y, z, p_x, p_y, p_z of this new 3×10^6 out-of-time proton beam.

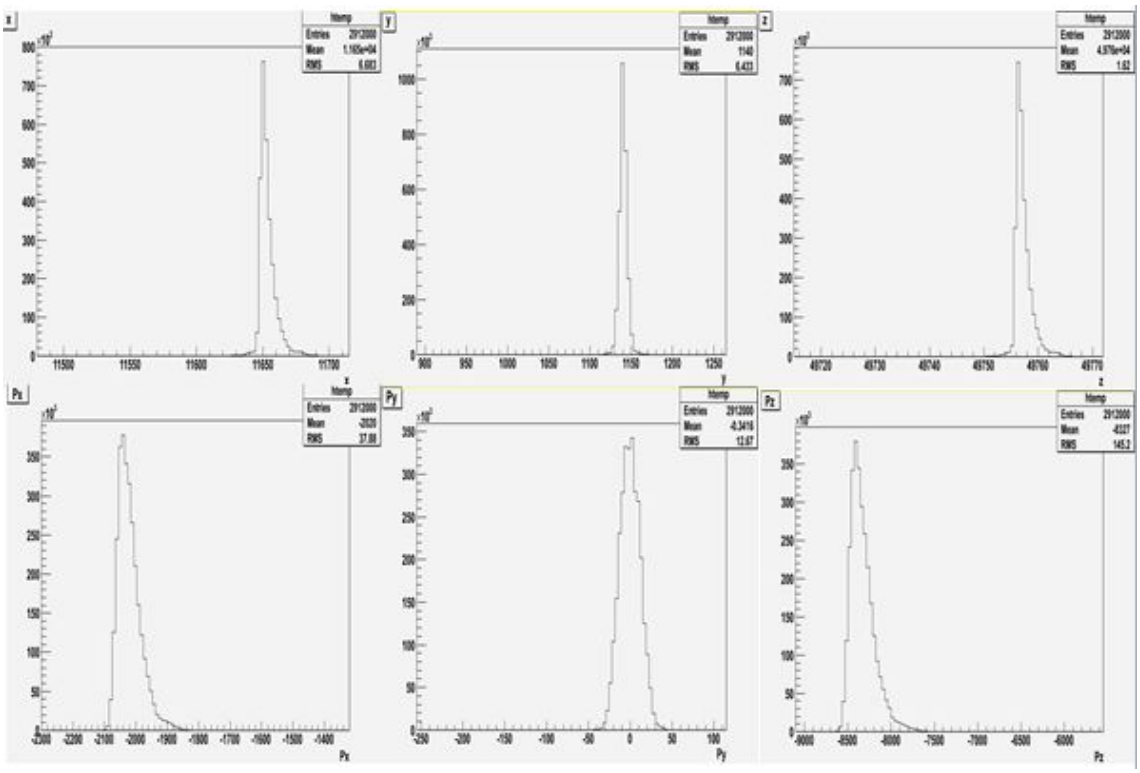

Figure 4.3: The x, y, z, p_x, p_y, p_z of the 3×10^6 events that were created incident on the target. The x-axis is in millimeters for x, y, z and in MeV/c for p_x, p_y, p_z.

The 3×10^6 protons were run through G4beamline with a few geometry modifications, all contained in a single file labeled BField9.txt.

4.3 Geometry

The geometry used for the simulations is the same geometry package used for regular G4beamline modeling, except with the addition of BField9.txt file. This text file contains three different groups of files. The first group contains a field map that consists of field values specified on a 3D grid describing the magnetic field in the Detector, Production, and Transport Solenoids. The second group of files cover the Proton Beam Absorber and the Extinction Monitor area. These files are touching but not overlapping with the other magnetic field files. The second group of files have a coarser grid than the first group, but these regions also have a shallow gradient so a coarser map is adequate. The third group of files cover the region of the extinction monitor. The 9 in BField9.txt stands for Mau9. This field map release modifies the angle of 16 coils of the second curve to have the beam better centered with respect to the Detector Solenoid axis [20].

4.4 Random Generator

After the 3×10^6 protons were created, they were run on approximately 1,900 worker nodes on Fermilab's Grid. To ensure that each out-of-time beam generated did not compile the same results, a random seed generator was introduced in both the Grid script and the G4beamline submission. The random seed was based on the day's date and time to insure that each submission to a worker node was unique. This allowed hundreds of jobs to be submitted at one time because they would remain statistically independent and the results could later be combined into one histogram. If a random seed had not been introduced, the jobs would have had to be submitted one at a time to take advantage of Grid's natural random generator. Groups of 300 and 500 jobs were submitted at a time to Fermilab's Grid

because of their completion time of approximately 12 hours. These were submitted primarily at night to reduce the interference with other jobs using Grid resources. In total, 5.7×10^9 protons were simulated, corresponding to 3×10^{13} protons prior to the AC dipole.

4.5 Virtual Detectors

There were four virtual detectors used with this simulation. Virtual detectors are detectors that do not actually exist in the Mu2e experiment but can be introduced in G4beamline in order to gauge the behavior of particles at a specific point in the experiment. One of these detectors (the Origin) G4beamline naturally creates, which shows where a particle is created. The x, y, z, p_x, p_y, p_z for the virtual detector Origin is shown in Figure 4.4.

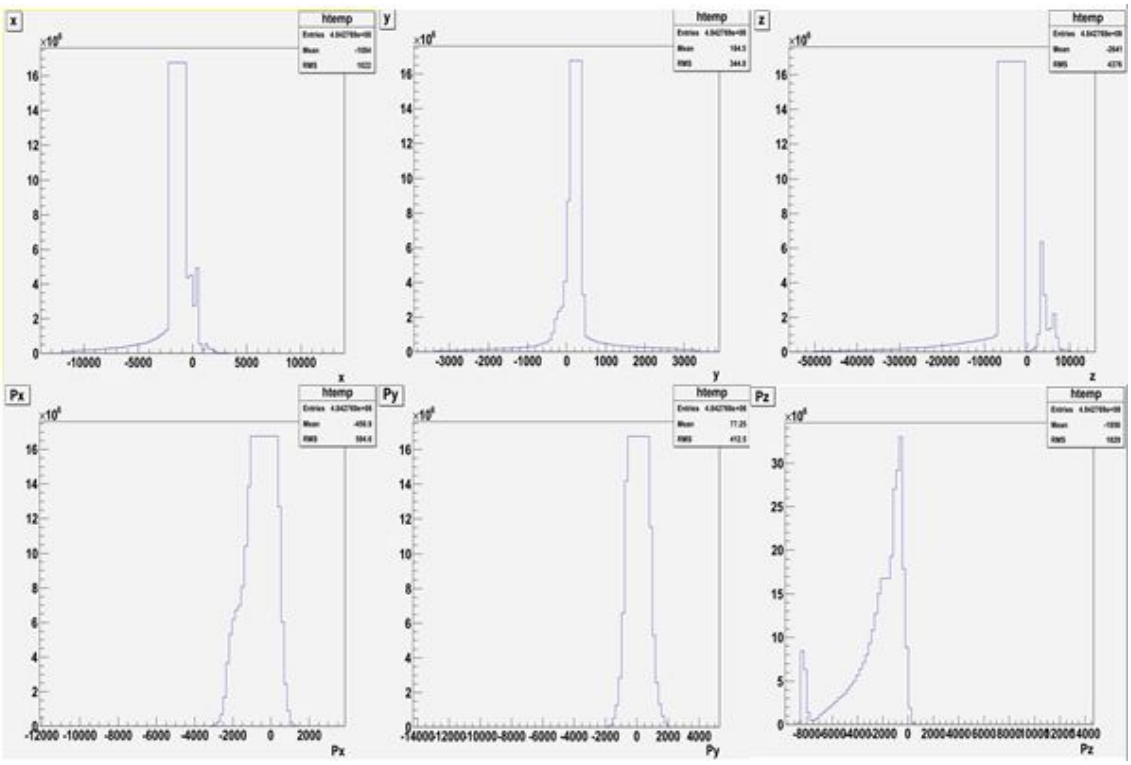

Figure 4.4: The x, y, z, p_x, p_y, p_z of each particle created. The x-axis is in millimeters for x, y, z and in MeV/c for p_x, p_y, p_z.

The second virtual detector was labeled "Start" and shows the behavior of the particles when the out-of-time proton beam is traveling towards the Production Solenoid. This detector had a length of 1 mm, a height and width of 100 mm, and was placed directly in the path of the proton beam. The x, y, z, p_x, p_y, p_z for the virtual detector Start, showing the initial proton beam traveling towards the production target, is shown in Figure 4.5.

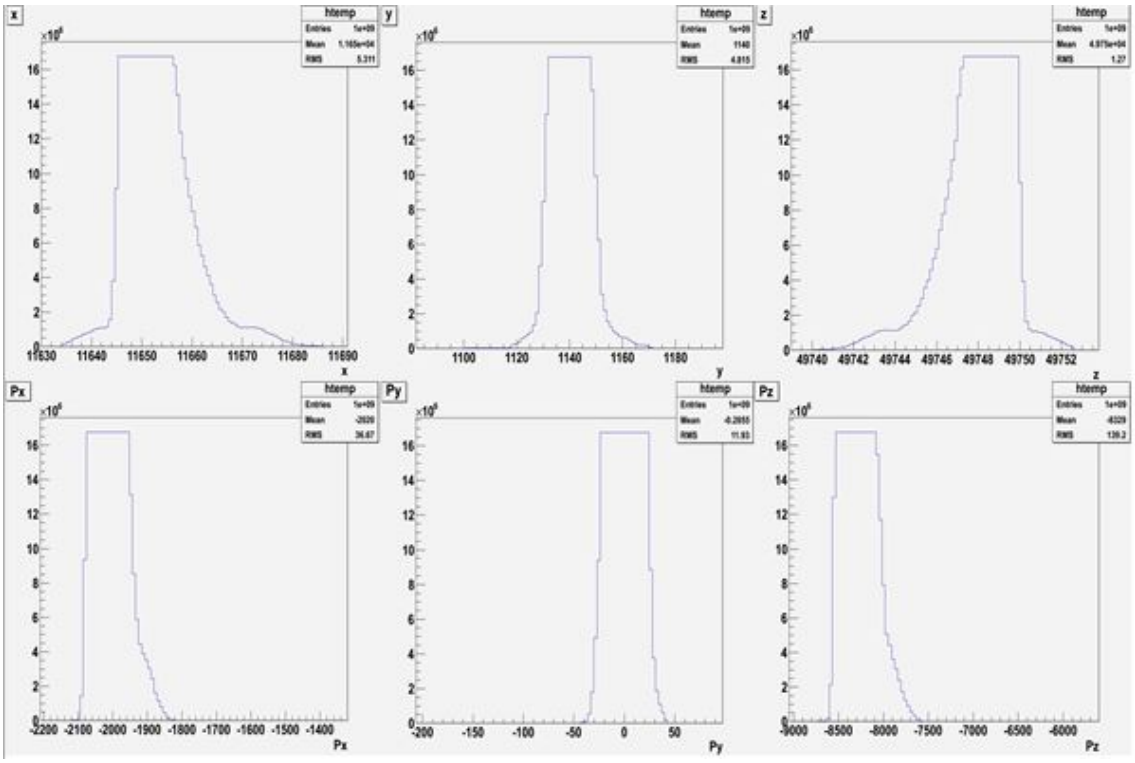

Figure 4.5: The x, y, z, p_x, p_y, p_z of the initial proton beam incident on the production target. The x-axis is in millimeters for x, y, z and in MeV/c for p_x, p_y, p_z.

The third virtual detector was placed around the production target. This detector showed how many out-of-time protons would interact with the production target and would have the potential to create an assortment of particles including muons, pions, and photons. This detector had a length of 180 mm, a radius of 3.15 mm, and was placed at 0,0,1842 mm in the simulation's coordinate frame. There were 1×10^7 out-of-time protons that interacted with the production target. The x, y, z, p_x, p_y, p_z for the virtual detector Target is shown in Figure 4.6.

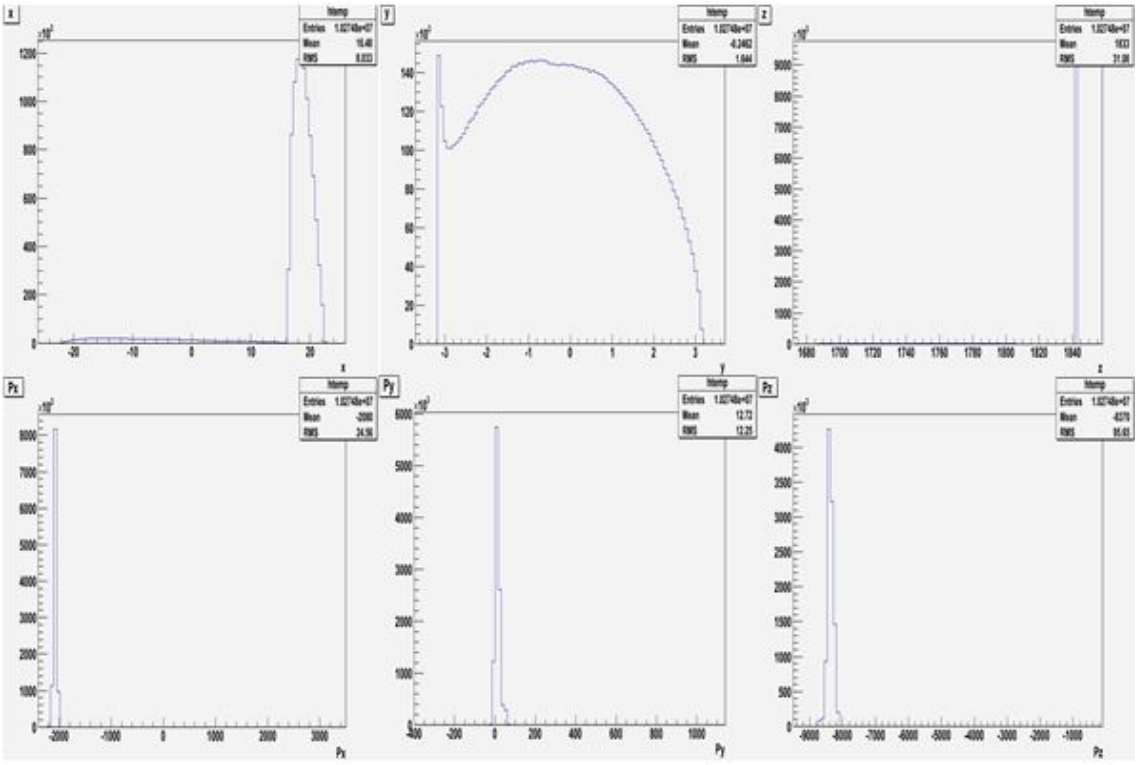

Figure 4.6: The x, y, z, p_x, p_y, p_z of the out-of-time protons that interacted with the production target. The x-axis is in millimeters for x, y, z and in MeV/c for p_x, p_y, p_z.

The final virtual detector was placed in front of the target extinction monitor system. This virtual detector showed how many particles would make it to the extinction monitor and potentially create tracks in the detectors simulating fake physics events. This detector had a length of 1 mm, a height and width of 200 mm, and was placed over the entrance to the target extinction monitor. Of the 5.7×10^9 protons incident on the production target, 3×10^5 particles went into the target extinction monitor. The x, y, z, p_x, p_y, p_z for the virtual detector Monitor is displayed in Figure 4.7.

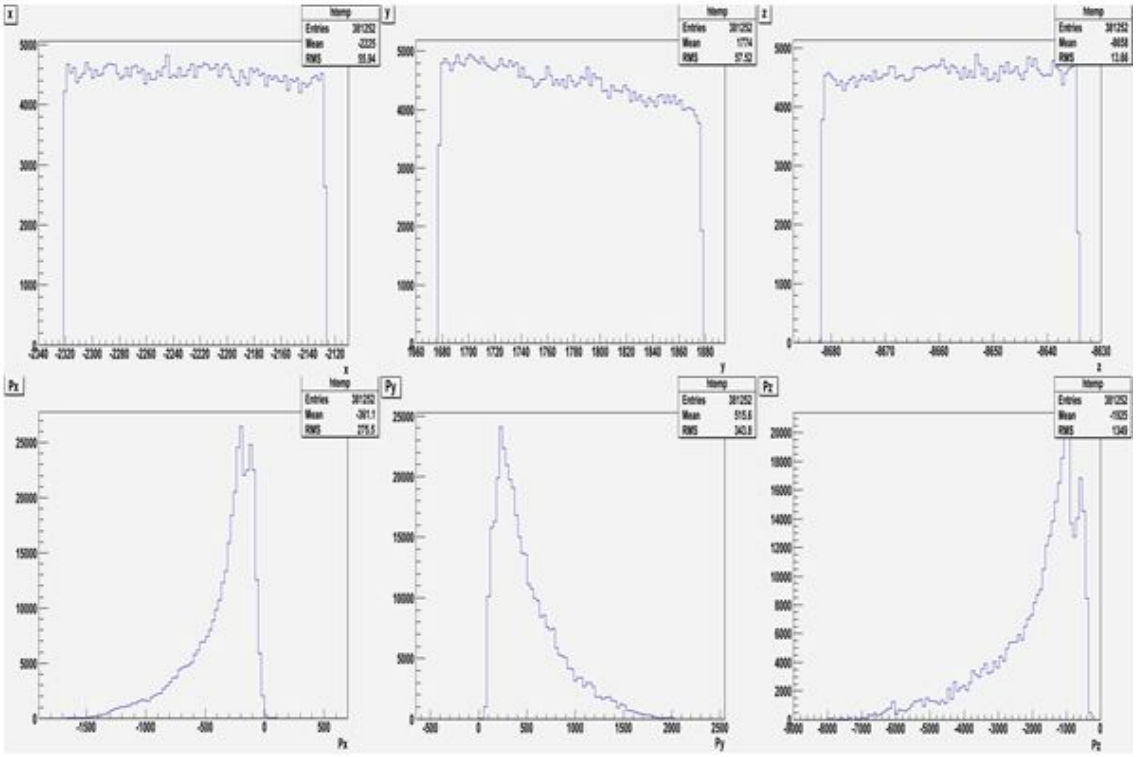

Figure 4.7: The x, y, z, p_x, p_y, p_z of the particles that went into the extinction monitor. The x-axis is in millimeters for x, y, z and in MeV/c for p_x, p_y, p_z.

4.6 Results

After compiling all 1,900 jobs, it was found that of the 1×10^9 events generated, 1×10^7 particles interacted with the production target and 3.8×10^5 made it to the target extinction monitor. These events were extracted and run through the target monitor with four virtual detectors in the filter magnet and a virtual detector for each scintillator in the pixel detector. Ultimately, it was shown that zero particles from the out-of-time proton beam off-target interaction made it through the filter magnet, much less left a signal. The dipole magnet in the extinction monitor is oriented to only transport charged particles with an average

p_z momentum of 4.2 GeV/c. The majority of the particles had a momentum less than 4.2 GeV/c and were removed. The extinction rate before the AC dipole is already 10^{-5}. Only 3000 of Prebys original 10^8 out-of-time protons were incident on the production target. If it is assumed one of these protons left a track in the extinction monitor, that would give the acceptance per 3×10^{13} protons prior to the AC dipole. This needs to be compared to the acceptance of 10^{-6} for normal beam protons giving a relative rate for out-of-time background of $10^{-5} \times (0.3 \times 10^{-14}) \div 10^{-6} = 0.3 \times 10^{-13}$, or 95% confidence level of less than 10^{-13}. Measurement of extinction at the 10^{-10} level is achievable.

CHAPTER 5

ANALYSIS OF PMT PERFORMANCE

At the upstream extinction monitor, Cherenkov counters (which consist of a radiator and photodetector) detect light from secondary particles produced by the beam-foil interaction. To build a beam time profile, low fake responses (after pulses) are needed in the photomultiplier tubes.

Several tests have already been preformed on PMTs by the NICADD group at Northern Illinois University. Cosmic rays were used to test several radiators: fused quartz GE type 021, UV transparent PMMA, and Cherenkov plastic EJ-299-15, as well as the photodetectors Hamamatsu PMT R7056 and FEU-115M [15]. After tests were completed, several preliminary decisions were made.

- A Hamamatsu R7056 would be the PMT used because of its UV glass window which provides an advantage in being able to register Cherenkov light.

- A custom made tapered voltage divider is desired to achieve a lower value for the PMT factory anode load. If the anode load is low, about 50 Ω, then there will be a few millivolt reduction in the last PMT stage if the anode current is large. In addition, the 50 Ω anode load will remove possible output pulse reflections [15].

- Silicone optical grease improves the optical connection between the Cherenkov radiator and the PMT input window allowing greater amplitudes.

For the upstream extinction monitor, there are 4 Cherenkov counters in coincidence with one another. In order to create a noise track, after pulses from the in-time beam must have

a coincidence in 3 out of 4 of the counters. One of the goals of this thesis is to study the after pulse rate and determine ways to reduce it. This was done by looking at a Hamamatsu R7056 PMT from the voltage range of 1.0 kV to 1.3 kV and using two custom resistors between the photocathode and the first dynode.

5.1 Setup

A cosmic ray stand situated 3 Cherenkov counters directly over one another in a vertical assembly. The top (Ch 4) and bottom (Ch 2) counters were in coincidence with one another. This means that when a cosmic ray triggered a pulse in both of these counters at the same point in time, a fictional pulse was generated in a virtual Cherenkov counter (Ch 3) on the oscilloscope. Whenever Ch 3 had one "true pulse", the PMT located in the middle of the assembly (Ch 1) was read out and stored for later analysis. The term "true pulse" signifies a large amplitude from a cosmic ray and not just generated noise. Likewise, the term after pulse means an additional trigger that results from electrons ionizing the gas impurities in the PMT hundreds of nanoseconds after the main pulse.

The counter under the test was located between the top and bottom counters. The counter consisted of a Hamamatsu PMT R7056 with a custom made voltage divider (voltage distribution ratio B, tapered) connected to a 12.7 mm thick UV PMMA radiator. When the negative voltage supply was 1 kV, the average divider current was about 2.5 mA.

Ch 4 was also a Hamamatsu PMT R7056 with the factory voltage divider (voltage distribution ratio B, tapered) connected to a 9 mm thick quartz radiator. This counter was connected to the positive power supply and had an average divider current of 0.25 mA with a 1 kV supply voltage.

Ch 2 was the bottom counter, a Hamamatsu PMT R6427 with the factory voltage divider (voltage distribution ratio A) connected to a 12.7 mm thick quartz radiator. This counter was connected to the positive power supply and had an average divider current of 0.21 mA with a 1 kV power supply. A schematic of the Cherenkov radiator setup can be seen in Figure 5.1 along with the actual setup in Figure 5.2. All radiators were about 100 mm long and 28 mm wide.

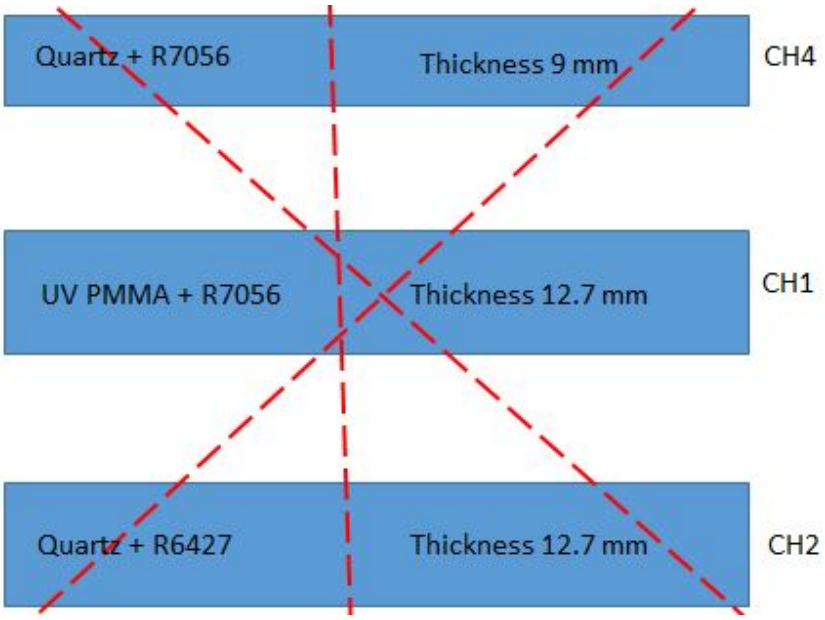

Figure 5.1: Setup schematic for Cherenkov counters.

Figure 5.2: Picture of PMT's in their vertical assembly.

The Hamamatsu PMT R6427 has a borosilicate glass window with a spectral response from 300 to 650 nm. The Hamamatsu PMT R7056 has a UV glass window with a spectral response from 185 to 650 nm. Both PMT's have a wavelength of maximum response of 420 nm [21]. Optical grade silicone grease (EJ-550) was applied to all channels, with an optical transmission cutoff wavelength of 350 nm [22]. In addition, Ch 4 had a silicone rubber optical interface (EJ-560) which served to reduce the transmission of particles with wavelength less than 300 nm [23]. The counter under test had a 50 Ω anode load which is preferable at high rates as discussed earlier.

All the PMT outputs were connected to the amplifier Lecroy Model 612A. One output of each amplifier was connected to the oscilloscope inputs Ch 1, Ch 2, and Ch 4. The outputs of Ch 2 and Ch 4 were also connected to the discriminator LRS Model 621L and then to the coincidence LRS Model 622 which supplied the input for Ch 3 on the oscilloscope. The discriminator threshold was at 30 mV. The coincidence and discriminator output pulses had a width of 20 ns. Ch 2 and Ch 4 were also connected to a positive power supply at 1.1 kV. Ch 1 was connected to a negative power supply varying from 1.0 to 1.3 kV. The crate that

contained the amplifier, discriminator, and coincidence is displayed in Figure 5.3 along with the positive and negative power supplies in Figure 5.4.

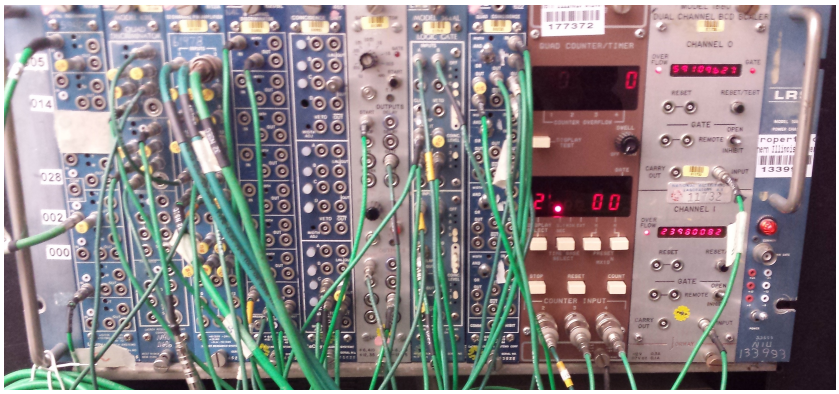

Figure 5.3: In order from left to right, the discriminator, amplifier, and coincidence models.

Figure 5.4: The positive and negative voltage power supply.

Each time a trigger was detected in Ch 3 (coincidence in Ch 2 and Ch 4), all four channels were displayed on the oscilloscope and subsequently saved to an output file by a NI Labview program. This program was originally written by Eric Johnson and later modified. A picture

of the oscilloscope with all four channels active is displayed in Figure 5.5. The time division is 200 ns.

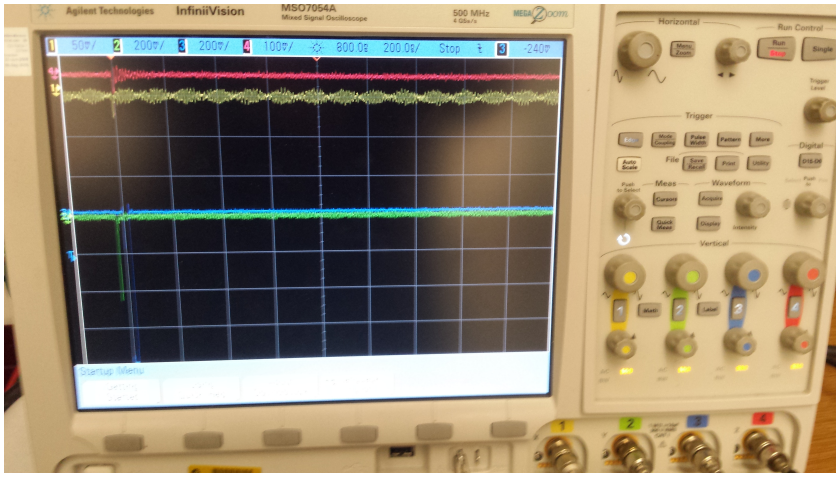

Figure 5.5: A picture of the oscilloscope with all channels active.

The rate of triggering was heavily dependent on the negative voltage being applied to Ch 1. At lower voltages, a significantly slower triggering rate was observed. At 1.3 kV, the triggering rate was approximately 200 events per hour. At 1.0 kV, the triggering rate was 30 events per hour.

5.2 Method

Data saved by Labview included the time the trigger occurred, the trigger number, a unique ID number, the channel, and data points collected every 2 ns over a 2000 ns time frame. Once this information was saved to an output file, it was later opened and read by a modified version of another NI Labview program written by Eric Johnson. This program allowed each channel's waveform to be analyzed and displayed in a virtual oscilloscope.

Data was collected over a 2000 ns time frame with the true pulse triggering at 200 ns and the after pulse triggering between 230 and 2000 ns. The 30 ns gap between the true

pulse and looking for the after pulse was introduced because occasionally there would be noise around the true pulse with enough amplitude to look like an after pulse.

The main goal of this study was to determine the best factors to lower the after pulse rate. This is a ratio of the number of true pulses to the number of after pulses. The methods under consideration were manipulating the power supply between 1.0 kV and 1.3 kV, and switching the resistor between the photocathode and the first dynode. The resistors used were 40 kΩ and 80 kΩ. A schematic of the Hamamatsu R7056 PMT voltage distribution ratio B is displayed in Figure 5.6.

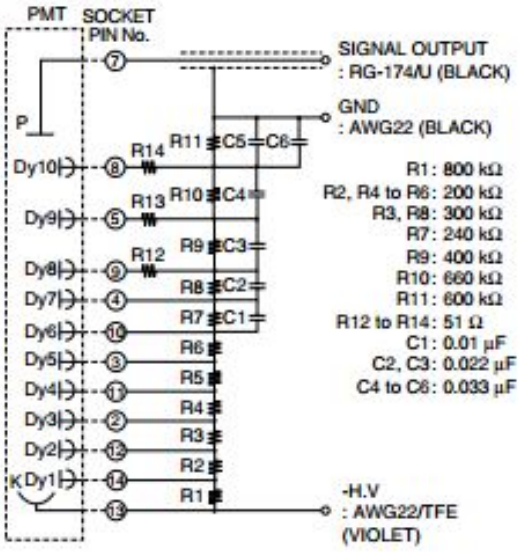

Figure 5.6: A schematic of the Hamamatsu R7056 voltage distribution ratio B.

All the resistors used in the PMT were 10× smaller than the values listed in the schematic with the exception of R12 to R14. R1 was the custom resistor that alternated between 40 kΩ and 80 kΩ. R15 is not listed in the schematic but is the tapered voltage divider of 50 Ω between the anode (socket pin number 7) and the shielding around the signal output. R12 to R14 were necessary in order to dampen the ringing around the true pulse. An actual Hamamatsu R7056 PMT is displayed in Figure 5.7.

Figure 5.7: A Hamamatsu R7056 PMT[21].

5.3 Comparing Resistors

A direct comparison between 40 kΩ and 80 kΩ voltages would not be an accurate assessment since the amplitude of the signal in the PMT is directly correlated to the current. As can be seen in Figure 5.6 above, the R7056 has multiple resistors all in series together. The equivalent resistance would be the summation of all the resistors. Ohm's law could then be applied to find the approximate current the PMT would be operating at with various combinations of first resistors and voltages. These calculations are shown in Table 5.1.

Table 5.1: Comparison of currents for different combinations of resitor and voltage

	40 kΩ			80 kΩ		
Total Resistance	320 kΩ			360 kΩ		
Voltage	1.0 kV	1.1 kV	1.2 kV	1.1 kV	1.2 kV	1.3 kV
Current	3.123 mA	3.435 mA	3.748 mA	3.054 mA	3.331 mA	3.609 mA

For closer comparison, similar currents in the 40 kΩ and 80 kΩ categories should be examined side by side.

5.3.1 Bad Events

The first step when analyzing data is to remove the bad events. Three criteria were used to define what a bad event was. The first criteria was that Ch 3 could only have one true pulse. If Ch 2 and Ch 4 had a large amount of noise, then it was possible to get multiple coincidences within the same 2000 ns. Having several triggers in Ch 3 resulted in a large amount of ringing in Ch 1. Both of these situations are displayed in Figures 5.8 and 5.9.

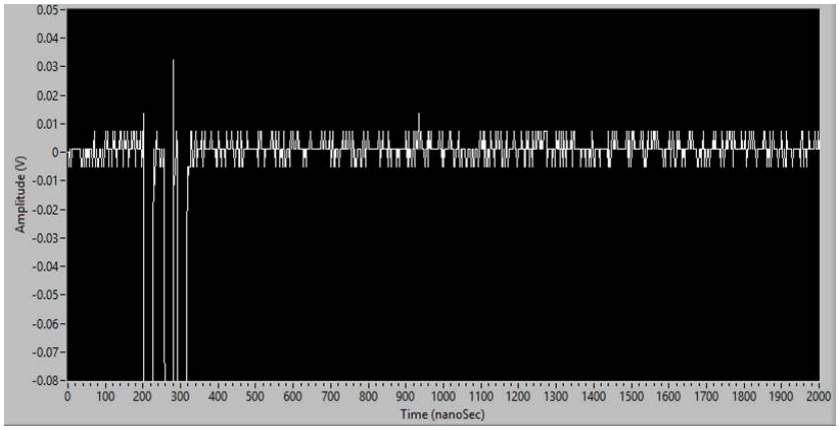

Figure 5.8: Ch 3 with multiple triggers.

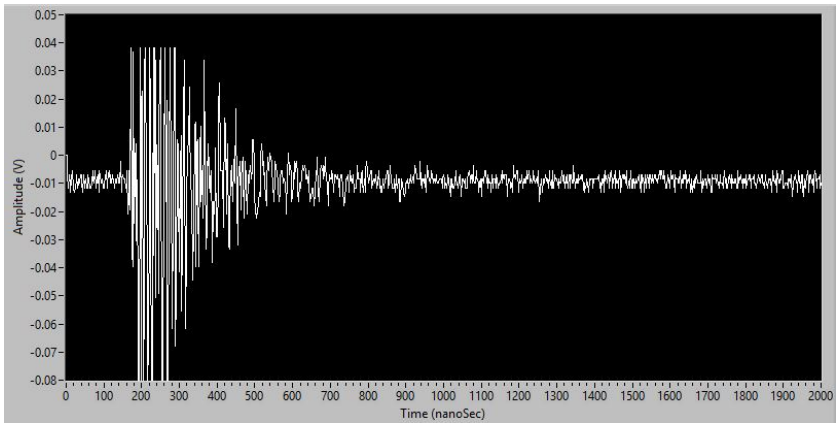

Figure 5.9: Ch 1 with ringing due to multiple triggers in Ch 3.

All waveforms in Ch 3 that had multiple minimum amplitudes smaller than -30 mV were detected, and removed, along with the corresponding waveforms in Ch 1, Ch 2, and Ch 4. The second criteria was that any waveform that had a positive amplitude greater than 20 mV was ringing and should be removed. The center of the waveforms were approximately -10 mV, so this criteria was actually detecting positive amplitudes of 30 mV or more.

Once the blatant bad events were removed, the final criteria was applied. This final criteria stated that any positive amplitudes detected greater than two standard deviations (2σ) was noise, and consequently, should be removed. The third criteria actually envelops the second, but distribution best fits were easier to determine and had a smaller error when steps were observed in this order. This process was done by writing a script in Matlab that accepted an input file of all Ch 1's data points and plotted them in a graph. Next, the script applied several distributions to the graph, including the Beta, Johnson SU, Laplace, Dagum 4P, Cauchy, Log-Logistic 3P, and many others. The Komogorov Smirnov, Anderson Darling, and Chi-Squared tests were used to determine the best fit. After the best fit was determined, the pedestal (center of waveform) and standard deviation were calculated with an average error of $\pm$ 0.5 mV. A summary of the bad events is displayed in Table 5.2.

Table 5.2: Summary of Bad Events

	40kΩ			80kΩ		
Voltages	1.0 kV	1.1 kV	1.2 kV	1.1 kV	1.2 kV	1.3 kV
# of Waveforms	780	19,205	14,600	19,965	18,030	19,340
Pedestal (mV)	-9.34	-9.59	-10.10	-9.34	-8.62	-9.11
σ (mV)	11.55	3.73	5.31	4.18	3.79	4.33
Pedestal + 2σ (mV)	13.76	-2.13	0.52	-0.96	-1.04	-0.45
Bad (Ch 3)	125	101	107	157	229	219
Bad (20 mV)	37	92	345	271	129	88
Bad (+2σ)	59	8596	3397	2899	6741	3692
% Bad	28.33%	45.76%	26.36%	16.66%	39.37%	20.68%

5.3.2 True Pulse and After Pulse

To determine the true pulse in Ch 1, the minimum was found before 230 ns. In order to qualify, the amplitude of the minimum had to be greater than 20 mV. In terms of the virtual oscilloscope, the minimum had to be further than 20 mV away from the pedestal of the waveform. A minimum amplitude threshold had to be applied since it was possible for there to be a coincidence in Ch 2 and Ch 4 yet still not have a true pulse in Ch 1. Figure 5.10 depicts the process of finding a true pulse in Ch 1, and Figure 5.11 shows that not every waveform has a true pulse.

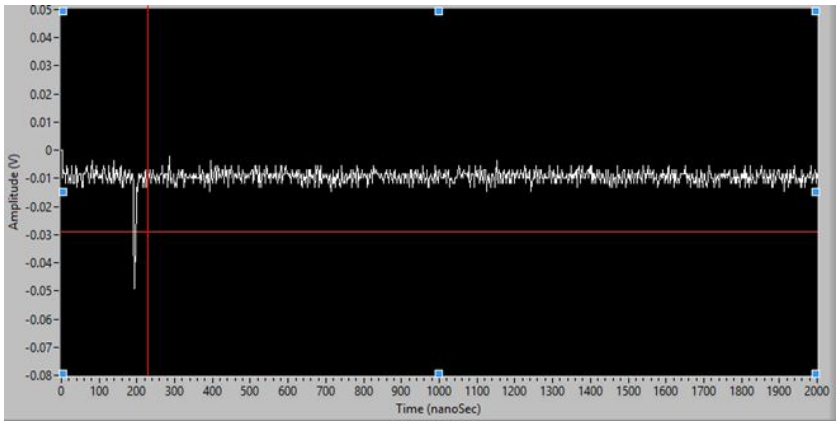

Figure 5.10: A true pulse is a minimum before 230 ns with an amplitude greater than 20 mV.

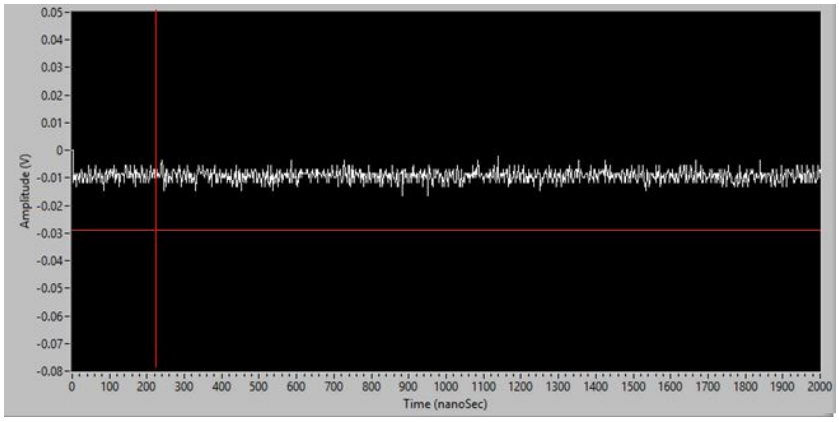

Figure 5.11: A waveform without a true pulse.

For the general graphs, the after pulse was simply the minimum after 230 ns with a data point below -12.5 mV on the virtual oscilloscope. Since the average pedestal was -9.35 mV, an after pulse only required an amplitude of 3.15 mV. Using this method, a minimum was collected for every waveform and later a threshold was applied to separate amplitudes. Figure 5.12 shows the requirements for flagging an after pulse.

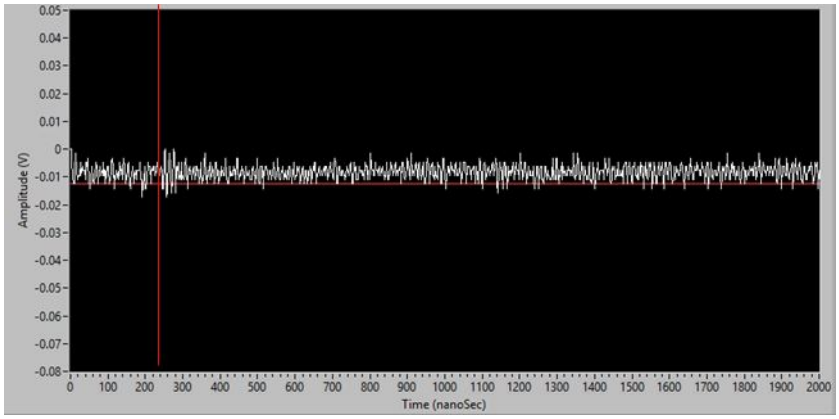

Figure 5.12: Collecting minimum for every waveform.

After all the minima were collected, amplitude vs frequency graphs for both the true pulse and after pulse were created. An example of 1.3 kV at 80 kΩ and 1.2 kV at 40 kΩ is displayed in Figure 5.13 and Figure 5.14.

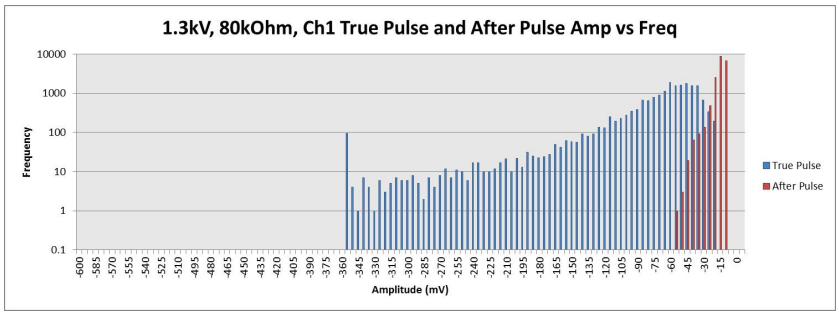

Figure 5.13: A graph of 1.3 kV, 80 kOhm, Ch1 True Pulse and After Pulse Amplitude vs Frequency.

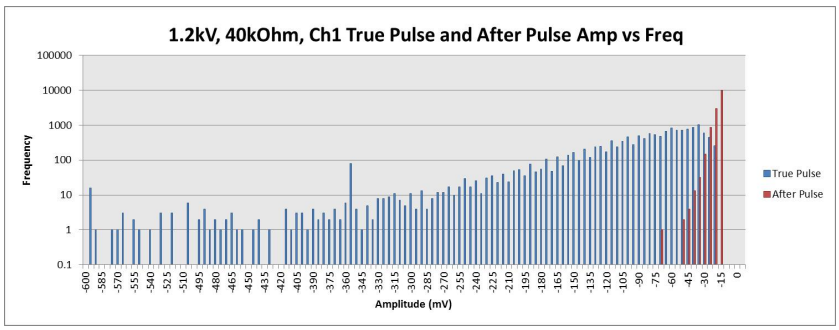

Figure 5.14: A graph of 1.2 kV, 40 kOhm, Ch1 True Pulse and After Pulse Amplitude vs Frequency.

Efforts were made to further define a pulse based on the wave distribution during the true pulse. If this could be determined, then it could be used to find true and after pulses in the Labview program instead of using minima and amplitudes. For the Hamamatsu R7056 PMT the true pulse is well defined as shown in Figure 5.15. The supply voltage is 1.5 kV, the rise time is 1.7 ns, the fall time is 4.5 ns, and the width is 2.0 ns [21].

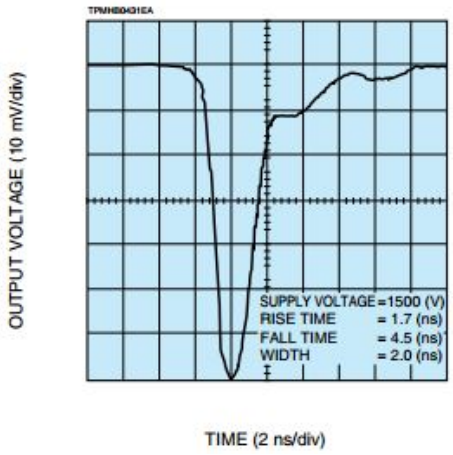

Figure 5.15: Anode output waveform of true pulse from Hamamatsu[21].

In order to have the most data points, a large amplitude was needed. To this end, true pulses for 80 kΩ at 1.3 kV were used. The largest minimum for a true pulse had an amplitude of 358 mV. There were 40 true pulses with this amplitude at the same point in time (192 ns). Several data points were recorded on each side of the minimum, giving a time range from 184 ns to 198 ns. These data points were all plotted together to determine if a pulse distruibtuion could be found. This graph is displayed in Figure 5.16.

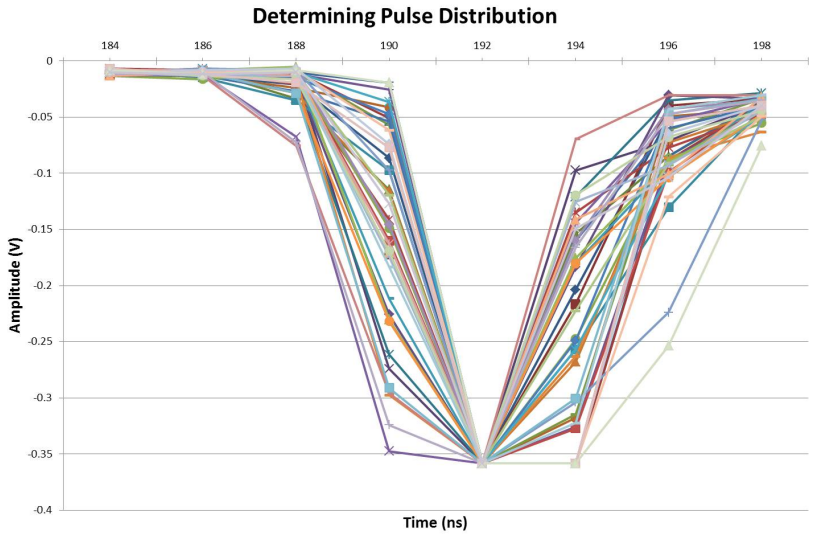

Figure 5.16: A graph of time vs amplitude in order to determine pulse waveform distribution.

Unfortunately, because of the large range of amplitudes on either side of the minimum, a best fit could not be determined. In the current setup, the true pulse only contained three data points. By decreasing the time per division on the oscilloscope, a better resolution of the true pulse could be obtained. It was determined that 0.5 ns per division would be needed to get a high enough resolution to determine a best fit. Doing this, however, reduces the time frame from 2000 ns to 500 ns, effectively obscuring 75% of the possible after pulses. While results of after pulses from the 200 ns to 500 ns range could be extrapolated, the current statistics are not high enough to do this with any accuracy. Using the current hardware setup, a pulse distribution cannot be determined.

5.4 Time Profile

A time profile was also built to detect any patterns that could emerge. Whenever a minimum was recorded, the time was also taken. The true pulse always occurred around 200 ns so only the after pulse minima were graphed. Figure 5.17 shows the time vs frequency for Ch 1, 1.3 kV, 80 kΩ. Amplitude was also added into the equation in order to get a different perspective. Figure 5.18 shows the correlation between amplitude, time, and frequency for Ch 1, 1.3 kV, 80 kΩ.

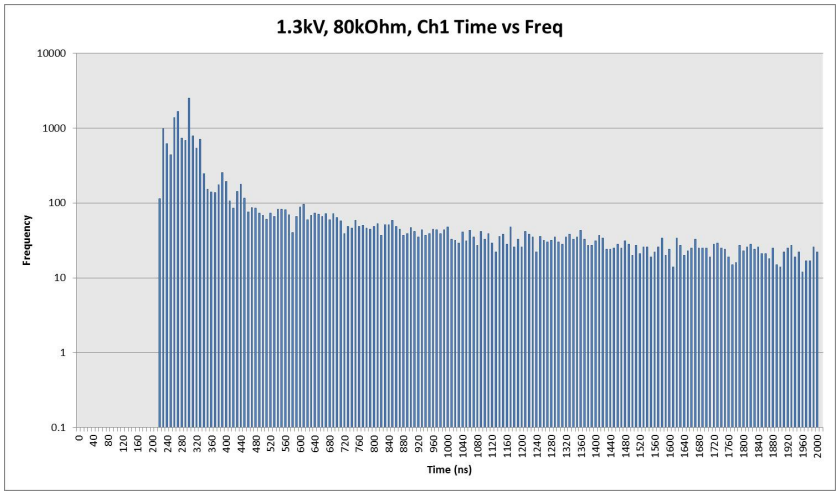

Figure 5.17: A graph of time vs frequency for Ch 1, 1.3 kV, 80 kΩ Frequency.

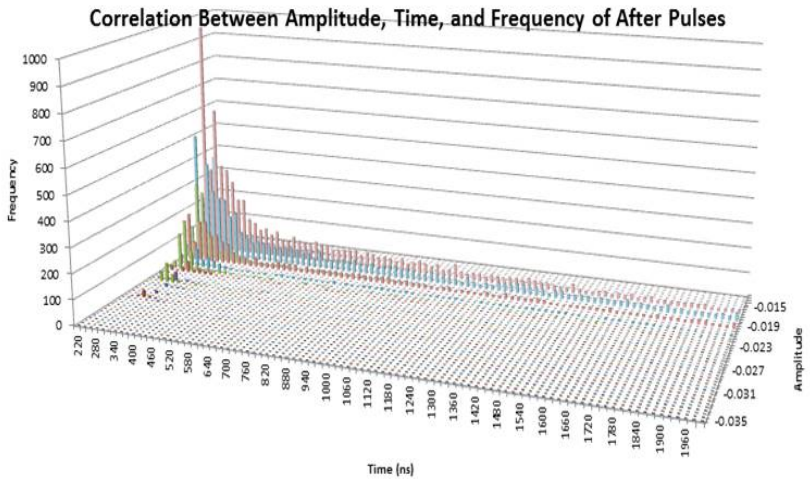

Figure 5.18: A graph of amplitude, time, and frequency for Ch 1, 1.3 kV, 80 kΩ.

5.5 Result

In order to finalize the results, a threshold was chosen for both the true pulses and after pulses to compare across voltages. It was decided that for the true pulse, it must have a 20 mV amplitude with respect to the pedestal (RTP). Because 2σ was used to ferret out bad events, using 20 mV as the amplitude guaranteed all minima were true pulses and not noise. The after pulse was defined as having an amplitude of 20 mV or greater, and then 30 mV or greater, with respect to the pedestal. All after pulses were checked by hand to confirm that they were actual after pulses. A complete summary of the after pulse rate is shown in Table 5.3. Waveforms - Bad is the number of waveforms left after the bad events had been removed from the initial count.

As can be seen in the table, lower voltages provide less after pulses. A smaller first resister lowers the after pulse rate as well. Unfortunately, it also lowers the amplitude of the true pulses as. For the best combination, a low resistor should be used with a large amplifier, magnifying the amplitude 20 - 30× the actual current. This would be 2 - 3×

Table 5.3: Summary of After Pulse Rate

	40kΩ			80kΩ		
Voltages	1.0 kV	1.1 kV	1.2 kV	1.1 kV	1.2 kV	1.3 kV
Waveforms - Bad	559	10,416	10,751	16,638	10,931	15,341
True Pulse (-20 mV RTP)	0	8,235	9,899	15,611	8,698	14,362
After Pulse (-20 mV RTP)	0	5	37	0	7	15
After Pulse (-30 mV RTP)	0	3	11	0	2	3
After Pulse Fraction (-20 mV)	0.00%	0.06%	0.37%	0.00%	0.08%	0.10%
After Pulse Fraction (-30 mV)	0.00%	0.04%	0.11%	0.00%	0.02%	0.02%

stronger than the setup currently at NIU. Another modification that could be made would be to manipulate R12 - R14 to get the optimal combination to reduce ringing around the true pulse.

All voltage and resistor combinations gave an after pulse rate less than 0.4%, which is well below what is needed for the upstream extinction monitor. In order to create a noise track in the telescope, there must be 3 out of 4 after pulse coincidences in the PMT's from a hit made by the in-time beam. If it is assumed that the after pulse rate is 0.01, but with a time window of 20 ns, that reduces it by a factor of 100 (so 1×10^{-4}), then for 3 out of 4 coincidences the rate would be $4 \times (1 \times 10^{-4})^3 = 4 \times 10^{-12}$ which is very low. Measuring extinction at the 10^{-5} level is possible with that level of after pulsing.

CHAPTER 6

CONCLUSION

This thesis showed that extinction of 10^{-10} is achievable with backgrounds from off-target interactions in the extinction monitor. With the methods already employed by Mu2e, a signal detection rate of 10^{-6} events per proton-on-target will result in approximately 2 out-of-time events per hour. Simulations were run that assumed a worst case scenario of 10^9 events incident on the production target. 1×10^7 particles interacted with the production target and 3.8×10^5 made it to the target extinction monitor. These events were extracted and run through the target monitor with virtual detectors in the filter magnet and at each pixel detector. Ultimately, zero particles traveled through the entire filter magnet, resulting in 0 tracks being generated in the pixel detectors. Compared to the in-time beam, a background of less than 10^{-13} was found from out-of-time interactions showing that extinction monitoring at the 10^{-10} level is achievable.

For the upstream extinction monitor, a 50 Ω resistor should be used at the anode/output signal junction so that at a large anode current there will be a few millivolt reduction at the last PMT stage. This anode load also serves to remove output pulse reflections. The after pulse rate was shown to be directly related to the voltage being applied to the PMT under the test. At lower voltages there are less after pulses. A lower first resistor also lowers the amount of after pulse rate. The measured after pulse rate is well below what is needed to measure a 10^{-5} extinction rate.

REFERENCES

[1] J. L. Hewett *et al.*, Fundamental Physics at the Intensity Frontier, 2012, arxiv:1205.2671v1[hep-ex].

[2] $https://upload.wikimedia.org/wikipedia/commons/0/00/Standard\_Model\_of\_Elementary\_Particles.svg$

[3] $http://www-sldnt.slac.stanford.edu/alr/standard_model.htm$

[4] Paul A. Tipler. *Elementary Modern Physics*, Worth Publishers, Inc., 1992.

[5] ATLAS collaboration (2012). *Observation of a New Particle in the Search for the Standard Model Higgs Boson with the ATLAS Detector at the LHC.* Physics Letters B 716 (1): 129. arXiv:1207.7214. Bibcode:2012PhLB..716....1A. doi:10.1016/j.physletb.2012.08.020

[6] F. Cei and D. Nicol *Lepton Flavour Violation Experiments.* Advances in High Energy Physics Volume 2014 (2014), Article ID 282915, 31 pages.

[7] The Mu2e Collaboration, Mu2e Conceptual Design Report, 2012, mu2e-doc-1169-v21.

[8] $http://mu2e.fnal.gov/how\_does\_it\_work.shtml$

[9] Lamm, Michael. Mu2e Production Solenoid Requirements Document. March 6, 2012. Mu2e-docdb-945.

[10] Lamm, Michael. Mu2e Transport Solenoid Requirements Document. March 17, 2012. Mu2e-docdb-947.

[11] Lamm, Michael. Mu2e Detector Solenoid Requirements Document. April 25, 2012. Mu2e-docdb-946.

[12] J. Beringer *et al.*, Phys. Rev. D 86, 010001 (2012).

[13] V.S. Pronskikh. Target Stations Design For The Mu2e Experiment. In *Proceedings of IPAC2014, Dresden, Germany*, ISBN 978-3-95450-132-8

[14] Hamamatsu. (1998, Jan) *Photomultiplier Tubes; Construction and Operating Characteristics, Connections to External Circuits*

[15] S. Boi, A. Dyshkant, D. Hedin, E. Johnson, E. Prebys, P. Rubinov. Hamamatsu PMT R7056 Study for the Extinction Monitoring System of the Mu2e Experiment at Fermilab. November 6, 2015. FERMILAB-CONF-15-456-AD-ND.

[16] N. Akchurin, H. Kim *A study on ion initiated photomultiplier after pulses* Nucl. Instr. and Meth. A574, 2007, pp. 121.

[17] Robert, Tom. Muons, Inc. *G4Beamline User's Guide*. November 2012.

[18] $http://www.fnal.gov/pub/science/computing/grid.html$

[19] E. Prebys. Beam Transmission and Extinction in the Mu2e Beam Line. July 9,2014. Mu2e-DOC-4054-v4

[20] $http://mu2e.fnal.gov/atwork/computing/BFieldMaps.shtml$

[21] $http://www.hamamatsu.com/resources/pdf/etd/R6427\_R7056\_TPMH1187E.pdf$

[22] $http://www.eljentechnology.com/images/stories/Data\_Sheets/Accessories/EJ550$ $\%20\%26\%20552\%20data\%20sheet.pdf$

[23] *http : //www.eljentechnology.com/images/stories/Data_Sheets/Accessories/EJ*560 %20*data*%20*sheet.pdf*